

Cavin1 intrinsically disordered domains are essential for fuzzy electrostatic interactions and caveola formation

Vikas A. Tillu¹, James Rae^{1,2}, Ya Gao¹, Nicholas Ariotti^{3,4}, Matthias Floetenmeyer², Oleksiy Kovtun⁵, Kerrie-Ann McMahon^{1,2}, Robert G. Parton^{1,2*} and Brett M. Collins^{1*}

1. The University of Queensland, Institute for Molecular Bioscience, St. Lucia, Queensland, 4072, Australia.
2. The University of Queensland, Centre for Microscopy and Microanalysis, St. Lucia, Queensland, 4072, Australia.
3. The University of New South Wales, Electron Microscope Unit, Kensington, New South Wales, Australia.
4. The University of New South Wales, Department of Pathology, School of Medical Sciences, Kensington, New South Wales, Australia.
5. MRC Laboratory of Molecular Biology, Cambridge Biomedical Campus, Cambridge, UK.

Running Title: Cavin1 disordered sequences in caveola formation

*Corresponding authors: Robert Parton, Ph: +61 (0)7 33462032, Email: r.parton@imb.uq.edu.au
Brett Collins, +61 (0)7 33462043, Email: b.collins@imb.uq.edu.au

Keywords – caveolae, Cavin, coiled-coil, intrinsically disordered protein, MURC, phase separation, PTRF, SDPR, SRBC, undecad repeat

Summary

Caveolae are spherical-structured nanodomains of the plasma membrane, generated by cooperative assembly of caveolin and cavin proteins. Cavins are cytosolic peripheral membrane proteins with negatively charged intrinsically disordered regions (DR1-3) that flank positively charged α -helical regions (HR1 and HR2). Here we show that the three DR domains of Cavin1 are essential for caveola formation and dynamic trafficking of caveolae. Electrostatic interactions between DR and HR regions promote liquid-liquid phase separation behaviour of Cavin1, assembly of Cavin1 polymers in solution, generation of membrane curvature in a reconstituted system, and Cavin1 recruitment to caveolae in cells. Removal of the first disordered region causes irreversible gel formation *in vitro* and results in aberrant caveola trafficking through the endosomal system. We propose a model for caveola assembly whereby fuzzy electrostatic interactions between Cavin1 proteins, combined with CAV1 and membrane lipid interactions, are required to generate membrane curvature and a metastable caveola coat.

Introduction

Caveolae (*'little caves'*) are membrane invaginations with a diameter of 50-60 nm that are abundant in the plasma membrane of many cell types such as muscle fibres, endothelial cells and adipocytes. These membrane nanodomains are important for an array of different functions including endocytosis, intracellular signalling, lipid and fatty acid homeostasis and response to membrane stress¹⁻³.

Although the precise details of caveola biogenesis remain enigmatic their assembly requires the activities of two families of proteins - caveolins and cavins - and their coordinated interactions with membrane lipids and cholesterol. The integral membrane proteins of the caveolin family (CAV1, CAV2 and muscle specific CAV3) are synthesized at the endoplasmic reticulum and trafficked via the Golgi apparatus to the plasma membrane⁴. Caveolins have an unusual hairpin structure that inserts into the membrane bilayer, with N and C-terminal domains exposed to the cytoplasm^{3,5,6}. When expressed on its own in mammalian cells the core caveolin CAV1 is diffusely localised in the plasma membrane and is unable to form spherical caveolae in the absence of cavins^{4,7}. However, CAV1 is able to generate membrane vesicles similar to caveolae (h-caveolae) upon heterologous expression in *Escherichia coli*⁸. This points to an intrinsic capacity of CAV1 to generate membrane curvature, which is thought to be enabled by the specific lipid composition of *E. coli* membranes. In metazoan cells however, the additional presence of the peripheral membrane cavin proteins is required for the formation of native caveolae. In particular, Cavin1 and CAV1 are together required and sufficient to generate a minimal core system for caveola formation at the plasma membrane, while other cavin family members require Cavin1 for their recruitment and are thought to provide regulatory or tissue-specific activities^{7,9,10}.

All cavin proteins share a highly characteristic domain architecture consisting of two core α -helical regions (HR1 and HR2) with relatively high sequence conservation^{11,12}. These are connected by three intrinsically disordered regions (DR1, DR2 and DR3), that possess very little sequence homology but share the property of being enriched in negatively-charged residues (**Fig. 1A**). Cavin proteins can assemble into homo- and hetero-oligomeric complexes that form a protein coat on the cytosolic face of caveolae; and the essential isoform Cavin1 can form homo-oligomers that drive caveola formation in the absence of other family members^{11,13,14}. The N-terminal α -helical HR1 domain of Cavin1 forms a core trimeric coiled-coil structure that also promotes heteromeric interactions between other members of the Cavin family¹¹. A surface exposed patch of basic amino acid residues in the HR1 domain has affinity for phosphoinositide lipid headgroups including phosphatidylinositol-4,5-bisphosphate (PI(4,5)P₂)¹¹. The C-terminal α -helical HR2 region of Cavin1 is unique in the cavin family as it also contains a stretch of repeated undecad sequences (11-mers) predicted to form a second coiled-coil structure termed UC1 (undecad of Cavin1)¹⁰. Basic amino

acids within the HR2 and UC1 domains can associate with phosphatidylserine (PS) to regulate caveola formation and stability¹⁰. These two α -helical lipid interacting sites are important for membrane recruitment and for generating caveolar membrane curvature. However, the molecular mechanisms of caveolar membrane association and higher-order assembly of Cavins with Caveolins at the cell surface are largely unknown.

In this study we examined the role of the uncharacterised DR domains of Cavin1 in caveola formation. The DR domains of Cavin1 are strictly required for caveola assembly, and a systematic dissection of these intrinsically disordered regions showed that there are minimal acidic sequences within the DR domains that are essential for caveolar targeting, *in vitro* membrane remodelling and homo-oligomeric Cavin1 complex assembly. We also show that Cavin1 undergoes electrostatically-driven self-association via its disordered regions that promotes liquid-liquid phase separation (LLPS) *in vitro*. Perturbing the DR domain-mediated dynamics of Cavin1 self-association has profound effects on Cavin1 and CAV1 localisation and caveolar trafficking in cells. Our results lead us to propose a model for caveola assembly involving ‘fuzzy’ electrostatic interactions by Cavin1 at the CAV1/membrane interface to generate a metastable caveola coat.

Results

Cavin1 forms electrostatically-driven polymers that depend on DR1 and DR3 domains

The cavin family proteins all share distinguishing structural similarities with each other, consisting of disordered N- and C-terminal domains DR1 and DR3, a central disordered region DR2, and interspersed α -helical coiled-coil region HR1 and predicted α -helical region HR2 (**Fig. 1A**). The trimeric coiled-coil HR1 domain and C-terminal HR2 domains are both rich in basic amino acid residues, while the three DR domains instead possess a high proportion of acidic amino acid residues. This alternating electrostatic charge distribution is a distinctive and conserved feature of all family members (**Fig. S1A**), indicating it is an essential characteristic of the proteins. We also used the D2P2 web server¹⁵ to analyse the sequence of Cavin1 for predicted regions of disorder, and confirmed that the DR1, DR2 and DR3 regions are predicted to be intrinsically disordered as suggested by previous secondary structure analyses^{10,11} (**Fig. S1B**). Interestingly, sites of phosphorylation in Cavin1 are predominantly found in the DR1, DR2 and DR3 domains, while sites of ubiquitylation are concentrated in the HR1 and HR2 regions. In subsequent experiments the boundaries of the mouse Cavin1 domains are defined as: DR1 (1-44), HR1 (45-155), DR2 (156-209), HR2 (210-310), and DR3 (311-392) (**Fig. 1A**). Expression constructs used in this study are outlined in **Fig. S2**.

We recently proposed that the predominantly negatively charged DR sequences of Cavin1 may associate with the positively charged HR domains to promote intra and/or inter molecular electrostatic interactions required for coat assembly¹². To probe the role of electrostatic interactions, we used fluorescence correlation spectroscopy (FCS) to measure the diffusional properties of purified GFP-tagged Cavin1 in both 500 mM NaCl (high salt) and 150 mM NaCl (iso-osmotic salt concentration). According to polymer theory, the diffusivity of protein molecules in solution decreases with increasing intermolecular interactions due to molecular crowding limiting its molecular motion¹⁶. GFP-Cavin1 (100 nM concentration) showed a remarkable decrease in its diffusivity with the reduction of ionic strength from 500 mM NaCl ($12.01 \pm 3.03 \mu\text{m}^2/\text{sec}$) to 150 mM NaCl ($4.02 \pm 0.50 \mu\text{m}^2/\text{sec}$) (**Fig. 1B**). This indicates that at physiological salt concentrations Cavin1 can form homomeric polymers with an average hydrodynamic radius ~ 55 nm, similar to those observed previously^{4,14}, and that this self-association is dependent on electrostatic interactions. In contrast to full-length Cavin1, removal of either N- or C- terminal DR1 or DR3 domains prevents this electrostatically driven self-assembly at lower physiological salt concentrations (**Fig. 1B**).

Next, we sought to understand the role of DR sequences in oligomeric assembly of Cavin1 in a more representative cellular milieu. For these experiments we used MCF7 cells, which lack caveolae and do not express any caveolin or cavin proteins^{14,17,18}. GFP-tagged Cavin1 proteins were transiently expressed and FCS analysis was used to measure the diffusivity of each protein in cell lysates (all at 150 mM NaCl). Full length GFP-Cavin1 in MCF7 cell lysates forms relatively

heterogeneous large molecular weight species in solution with slow diffusive properties ($6.35 \pm 2.35 \mu\text{m}^2/\text{sec}$) (**Fig. 1C**) similar to purified recombinant GFP-Cavin1. In contrast to purified recombinant GFP-Cavin1- ΔDR1 , the N-terminal DR1 deletion in cell lysates showed a similar (although tending to faster) rate of diffusion to the full-length protein ($7.65 \pm 4.40 \mu\text{m}^2/\text{sec}$) (**Fig. 1C**). Complete deletion of the C-terminal DR3 region of GFP-Cavin1- ΔDR3 however, significantly increased the diffusivity of Cavin1 in MCF7 lysates ($18.54 \pm 6.22 \mu\text{m}^2/\text{sec}$), similar to the recombinant GFP-Cavin1- ΔDR3 (**Fig. 1C**). Overall these studies demonstrate a role for the DR sequences in electrostatically-driven polymerisation of Cavin1 in solution.

Cavin1 undergoes liquid-liquid phase separation (LLPS) influenced by the DR domains

There is an increasing awareness of the role of intrinsically disordered sequences in generating membraneless organelles via liquid-liquid phase separation (LLPS) or ‘demixing’ of proteins and associated molecules in solution. Such demixing phenomena can be driven by a variety of different mechanisms, including cation- π and π - π stacking, interactions with polyanions such as RNA, and intermolecular electrostatic interactions¹⁹⁻²². A number of recent studies have shown that membranes can be platforms for nucleating and transporting phase-separated assemblies, or in turn be regulated and organised via LLPS-mediated processes²³⁻³⁴. It has also been proposed that the formation of phase-separated condensates can perform physical work on their surroundings, including at the membrane-cytosol interface to generate membrane curvature³⁵⁻³⁸. Because of the demonstrated importance of disordered regions in Cavin1 for its assembly behaviour, we decided to assess if purified Cavin1 is able to form supramolecular assemblies leading to LLPS *in vitro*.

Purified recombinant GFP-Cavin1 remains dispersed in solution at both iso-osmotic NaCl concentration (150 mM) and at high NaCl concentration (750 mM) within a protein concentration range of 1 to 10 μM (**Fig. S3A**). However, when Dextran T-500 (1.25% w/v) was added as a macromolecular crowding agent^{39, 40} GFP-Cavin1 rapidly formed spherical liquid droplets at 150 mM NaCl even at low protein concentrations (0.1 μM) (**Fig. S3B**). These droplets increased in size with increasing protein concentration in the range 1 to 10 μM (**Fig. 2A**). Increasing the salt concentration strongly inhibited the ability of GFP-Cavin1 to undergo LLPS, consistent with a role for electrostatic intermolecular interactions^{20, 41}. Deletion of the C-terminal DR3 domain had a small but reproducible effect on the tendency of GFP-Cavin1- ΔDR3 to undergo LLPS, with droplet formation showing greater sensitivity to increasing ionic strength and protein concentration (**Fig. 2A; Fig. S3B**). Deletion of the DR1 domain had a dramatic effect leading Cavin1 to transition into non-spherical coacervates at all protein and salt concentrations (**Fig. 2A; Fig. S3B**). Fluorescence recovery after photobleaching (FRAP) was used to analyse the diffusion of proteins within the liquid droplets and the ability of GFP-Cavin1 to exchange with bulk solution. GFP-Cavin1 ($\tau_{1/2} \sim 20\text{s}$) and

GFP-Cavin1- Δ DR3 ($\tau_{1/2} \sim 10$ s) showed rapid fluorescence recovery after photobleaching, indicating there is ready exchange of protein molecules as expected for liquid droplets (**Fig. 2B, 2C**). GFP-Cavin1- Δ DR1, however, showed virtually no recovery (**Fig. 2B, 2C**), suggesting that gel formation has occurred and the truncated protein is unable to diffuse within the condensates^{19,42}. Overall, these analyses highlight the importance of electrostatic interactions in promoting self-association and subsequent LLPS behaviour by Cavin1 *in vitro*, and suggest distinct roles of DR1 and DR3 sequences in this process.

The Cavin1 DR sequences are essential for membrane remodelling *in vitro*

We previously showed that Cavin1 and Cavin2 possess an intrinsic ability to tubulate artificial lipid membranes using negative stain electron microscopy¹¹. To examine this membrane remodelling by Cavin1 at higher resolution, we first performed cryoelectron microscopy (cryoEM) analysis of samples after mixing purified Cavin1 with small unilamellar vesicles (SUVs) composed of Folch lipid extracts. We observed formation of an extensive network of membrane tubules (34 ± 5 nm, 12 tubules, 2 independent experiments) possessing a Cavin1 protein coat using both negative stain electron microscopy and cryoEM (**Fig. 3A**). We also observed some smaller vesicles (20 ± 4 nm in diameter), suggesting that Cavin1 may have a capacity to induce membrane fission at sufficient concentrations *in vitro*. Examination of the Cavin1-coated tubules in three dimensions by cryoelectron tomography (cryoET) revealed a striated but relatively heterogeneous pattern of protein densities around the tubules (**Fig. 3B; Movie S1**). This is consistent with structures previously observed on the cytosolic face of caveolae using fast-freeze deep-etch^{43,44} and conventional EM methods⁴⁵⁻⁴⁷, and with the elongated rod-like structures of isolated Cavin1 observed by negative staining EM¹¹. These experiments indicate that Cavin1 possesses an inherent membrane remodelling activity, driven by polymeric assembly on the membrane surface.

The importance of Cavin1 DR domains in self-association and LLPS next raised the question as to whether they play a role in its key ability to physically remodel membranes. To this end, we used the *in vitro* membrane remodelling assay to investigate their importance in generating membrane curvature. We expressed and purified a range of Cavin1 DR domain truncations with an N-terminal His-ubiquitin (HisUb) tag (**Fig. 3C**) and used the membrane tubulation assay combined with negative stain EM to analyse their ability to remodel mammalian (Folch) synthetic phospholipid membranes (**Fig. 3D**). It was immediately apparent that complete removal of the N-terminal DR1 and C-terminal DR3 domains abolished the ability of Cavin1 to tubulate liposomes *in vitro*. Shorter truncations showed that while the N-terminal DR1 deletion Cavin1(10-392) still formed membrane tubules, these were relatively infrequent and of a smaller diameter (~ 10 nm), whereas further deletion of N-terminal DR1 sequences in Cavin1(30-392) prevented the formation of membrane tubules altogether. The C-

terminal DR3 deletion mutant Cavin1 (1-345) formed membrane tubules similar to full length Cavin1, with the minor caveat that we observed an increased number of smaller vesicles. However, the deletion of further amino acids from the C-terminus in Cavin1(1-330) completely inhibited membrane tubulation. For those DR truncation mutants that lacked membrane remodelling activity we observed instead a propensity to cause liposome clustering. This likely occurs because these Cavin1 constructs can now bind adjacent phospholipid vesicles via multiple positively charged surfaces of the HR1 and HR2 domains, unrestrained by compensating negatively-charged DR1 and DR2 sequences ¹¹. Overall, these studies define a core Cavin1 sequence (10-345) required for Cavin1 to efficiently promote membrane curvature.

We next examined the ability over time of purified GFP-Cavin1 to modulate giant multilamellar vesicles (GMVs) doped with 0.1 mol% fluorescent Bodipy-TMR PI(4,5)P₂ analogue. GFP-Cavin1 showed strong localised clustering at the membrane surface compared to other membrane remodelling proteins (**Fig. 4A**) ^{48, 49}, and possessed a remarkable membrane sculpting activity as indicated by the rapid collapse of GMVs over a period of several minutes (**Fig. 4B**). In contrast, although both the N- and C-terminal DR deletions of Cavin1 still bound efficiently to the GMVs, they did not display any significant membrane sculpting activity (**Fig. 4C, 4D**). With Cavin1- Δ DR1 we also often observed a characteristic accumulation of the protein at the interface between adjoining vesicles leading to the clustering of the GMVs (**Fig. 4E**). Overall, these studies using GMVs and SUVs show that while the DR1 and DR3 domains are dispensable for membrane binding, they have an essential role in the ability of Cavin1 to sculpt the curvature of phospholipid membranes.

Cavin1 disordered sequences are essential for interacting with CAV1 and forming caveolae

Our studies *in vitro* highlight several properties of Cavin1 that are dependent on its disordered sequences. Firstly, DR1 and DR3 of Cavin1 are important for the formation of polymers and LLPS promoted by electrostatic interactions, and the DR1 domain is required for the dynamic properties of Cavin1 in LLPS; removal of the DR1 domain results in gel formation and prevents its free diffusion within the condensates. The Cavin1- Δ DR1 construct also displays a capacity to bind and cluster membrane vesicles *in vitro*. Secondly, minimal sequences of Cavin1 DR1 and DR3 are required for membrane remodelling. To examine the importance of Cavin1 disordered N- and C-terminal domains to functional caveola formation, we next analysed the localisation of the DR1 and DR3 truncation mutants in cells (**Fig. 5A**). The prostate cancer PC3 cell line was used, which expresses CAV1 but does not express any members of the Cavin family so that CAV1 is diffusely localised at the plasma membrane ^{7, 9}. Expression of full-length GFP-Cavin1 in PC3 cells fully restores the formation of caveolae with CAV1 (in the absence of other cavins), providing a functional readout for Cavin1 activity ^{7, 9, 10, 50}. Using either standard confocal microscopy (**Fig. S4A**) or confocal fluorescence with

Airyscan super-resolution imaging (**Fig. 5A**), full length GFP-Cavin1 showed the characteristic punctate distribution and co-localised with CAV1 at the plasma membrane. In contrast, after removal of the C-terminal domain GFP-Cavin1- Δ DR3 is unable to promote caveola formation and now accumulates in the cytosol and also associates extensively with microtubules (**Fig. 5A, Fig. S4B**). This is consistent with a previous report of a similar C-terminal truncated Cavin1 (residues 1-322) in CHO cells⁵¹. FRAP analysis of GFP-Cavin1- Δ DR3 on microtubules showed a fast fluorescence recovery, indicating a dynamic exchange with the cytoplasm or diffusion along the microtubules (**Fig 5B, Movie S2**). Interestingly, when microtubules were depolymerised with nocodazole this resulted in redistribution and condensation of GFP-Cavin1- Δ DR3 to form spherical droplets in the cytosol. These also showed fast exchange of protein molecules with the bulk cytoplasm suggestive of liquid-droplet behaviour (**Fig. 5C, S3B, Movie S3**). This suggests a dynamic equilibrium exists between cytosolic, liquid droplet and microtubule associated states of the GFP-Cavin1- Δ DR3 truncation.

Strikingly, expression of GFP-Cavin1- Δ DR1 resulted in the formation of large intracellular structures that also contained endogenous CAV1 (**Fig. 5A, S4A**). A C-terminal tagged Cavin1- Δ DR1-GFP construct showed similar clusters co-localised with CAV1, confirming this phenotype is not influenced by the location of the GFP tag (**Fig. S4C**). To analyse these structures in more detail, we performed co-localisation experiments of GFP-Cavin1- Δ DR1 with various cellular markers. While no overlap was seen with the Golgi complex, lysosomal or recycling endosomal membrane markers, a significant proportion of GFP-Cavin1- Δ DR1 and endogenous CAV1 were found to colocalise with the early endosomal marker EEA1 (**Fig. S5A**). Airyscan microscopy revealed that clusters of EEA1 positive endosomes surrounded the GFP-Cavin1- Δ DR1 and CAV1 positive structures (**Fig. 5D; Fig. S5B**). These were visualised by APEX labelling and electron microscopy imaging⁵² of GFP-Cavin1- Δ DR1 in PC3 cells, revealing intracellular assemblies consisting of large tethered vesicular clusters with a surrounding halo of GFP-Cavin1- Δ DR1 labelling (**Fig. 5E**). In contrast, GFP-Cavin1 expression resulted in formation of the characteristic single caveolae and rosettes of caveolae at the plasma membrane as expected (**Fig. 5E**).

We finally performed live imaging of PC3 cells expressing either GFP-Cavin1 or GFP-Cavin1- Δ DR1 with Rab5a-mCherry as a marker of early endosomes. Caveolae are consistently localised to the trailing edge of migrating cells, where constant membrane remodelling events are occurring⁵³. In migrating PC3 cells we observe dynamic GFP-Cavin1 positive caveola puncta undergoing transient fission and fusion events and kiss-and-run interactions with Rab5a-mCherry positive endosomes similar to previous observations⁵⁴ (**Fig. 5F, Movie S4**). In contrast, GFP-Cavin1- Δ DR1 initially showed plasma membrane puncta fusion events similar to GFP-Cavin1 (imaged at an early 12 h time point following transfection before larger immobile condensates are formed), but over

time resulted in formation of the larger structures that stably associated with Rab5a positive endosomes (**Fig. 5F**, **Movie S5**). This suggests that the DR1 domain is important for the dynamics of intracellular trafficking and recycling of caveolae at endosomes. Overall, our results show that disordered sequences of Cavin1 are essential for generating caveolae, but that each DR domain has a distinct function. Removing the C-terminal DR3 domain prevents interaction with CAV1 and results in mis-localisation to the cytoplasm and association with microtubules. Removing the N-terminal DR1, which results in gel formation and membrane clustering *in vitro*, allows initial caveolae puncta formation at the plasma membrane, but then causes subsequent accumulation of aberrant intracellular protein and membrane assemblies with a subset of early endosomes unable to recycle to the plasma membrane.

Minimal Cavin1 DR sequences needed for membrane remodelling are also essential for caveola formation

Using the same series of truncations tested *in vitro* for membrane remodelling activity, we next asked if the same minimal sequences are sufficient for caveola formation in cells. GFP-Cavin1(10-392) with deletion of the first nine amino acids showed a relatively normal localisation with CAV1 puncta at the cell surface. However, GFP-Cavin1(30-392) formed large intracellular puncta and clusters that co-localised with CAV1 (**Fig. 6A**), and also showed a partial co-localisation with EEA1 (**Fig. S5C**), similar to Cavin1 with the complete DR1 domain removed. Thus, deletion of the N-terminal DR1 sequence of Cavin1 has a progressive effect on the re-distribution of caveolae from the plasma membrane to intracellular endocytic compartments.

The C-terminal DR3 truncation GFP-Cavin1(1-345) retained a normal ability to generate plasma membrane puncta that co-localised with CAV1 (**Fig. 6A**), and APEX labelling and electron microscopy of GFP-Cavin1(1-345) showed its normal localisation to caveolae at the plasma membrane (**Fig. 6B**). Further deletion of C-terminal DR3 sequences in GFP-Cavin1(1-330), however, resulted in a total cytosolic redistribution. The C-terminal truncations show that amino acids (346-392) are mostly dispensable for generating caveolae in PC3 cells, while residues 330-345 are essential. Finally, we used a proximity ligation assay (PLA)¹⁰ to assess the interactions of Cavin1 C-terminal truncations with CAV1 at the plasma membrane. PLA analyses correlated with the cellular imaging of the GFP constructs, showing that the mutant Cavin1(1-345) can interact with (or is at least in close proximity to) CAV1, while the shorter truncations Cavin1(1-330) and Cavin1(1-310) do not (**Fig. 6C**).

Specific DR sequences are essential for the ability of Cavin1 to form caveolae

The sequences 1-30 and 310-345 in DR1 and DR3 are required for Cavin1 to efficiently remodel synthetic phospholipid membranes *in vitro*, and for caveola formation with CAV1 in cells. To understand these sequences in more detail we generated several specific DR domain mutants in the context of the minimal functional construct Cavin1(1-345) (**Fig. 7A**; **Fig. S6A**). We first tested whether the acidic amino acids of the disordered sequences were important by mutating the Glu/Asp residues in either DR1 or DR3 regions to alanine (M1 and M3 respectively). We also tested the acidic residues in the central DR2 region (mutant M5). By FCS, all three variants showed a significant increase in diffusivity with respect to wild-type Cavin1(1-345), indicating that their net negative charge is important for self-association (**Fig. 7B**).

When GFP-tagged Cavin1(1-345) mutant M1 was expressed in PC3 cells it formed large intracellular puncta and co-localised with CAV1 (**Fig. 7C**). These puncta also colocalised with a sub-population of EEA1-positive endosomes, but not LAMP1 or GM130 (**Fig. S6B**). APEX labelling and imaging by EM showed clusters of GFP-Cavin1(1-345) mutant M1 that appeared identical to those formed by either GFP-Cavin1- Δ DR1 or GFP-Cavin1(30-392) (**Fig. S6C**). The GFP-tagged Cavin1 mutants M3 and M5 in contrast both showed a diffuse cytosolic localisation in PC3 cells (**Fig. 7C**). These results show that the acidic Glu/Asp residues in the Cavin1 DR1, DR2 and DR3 domains are all essential for forming caveolae with CAV1 at the cell surface. The acidic side-chain mutations M1 and M3 respectively result in identical phenotypes to the complete deletion of the entire DR1 or DR3 domains.

We next assessed two additional mutants, where the DR1 or DR3 domains were substituted with random Gly/Ser sequences while maintaining the relative positions of acidic Asp/Glu residues and prolines (M2 and M4 respectively) (**Fig. 7A**; **Fig. S6A**). The objective was to determine if any other sequences apart from the acidic side-chains contributed to the activity of these domains. In MCF7 cell lysates neither the M2 or M4 mutant showed a major difference in diffusivity by FCS compared to wild-type Cavin1(1-345) indicating that only the acidic side-chains are necessary for self-association (**Fig. 7B**). Furthermore, the subcellular localisation of GFP-Cavin1(1-345) mutant M2 in PC3 cells showed normal co-localisation with CAV1 at the plasma membrane (**Fig. 7C**), indicating that it is the electrostatic properties of the sequence from 1-30 that is important for function and not the specific sequence itself. In contrast however, despite its normal ability to self-associate, the mutant M4 is unable to restore caveola formation with CAV1 in PC3 cells (**Fig. 7C**; **Fig. S6D**). Instead we observe the formation of numerous spherical cytoplasmic structures, that dynamically exchange with the cytosol as shown by FRAP analysis and regularly undergo fusion, suggesting the protein has undergone LLPS and droplet formation (**Fig. 7D**, **Movie S6**). Remarkably, unlike the complete DR3 deletion however, purified Cavin1(1-345) mutant M4 is still able to remodel and tubulate synthetic liposomes *in vitro* (**Fig. S6E**). This indicates that specific sequences in the Cavin1

region 310-345 are dispensable for polymer formation, LLPS and membrane remodelling, but are essential for recruitment to caveolae with CAV1 in cells. The acidic side-chains in this region, however, are required for all of these functional Cavin1 activities. Altogether, these studies demonstrate the critical importance of acidic residues in all three DR domains for promoting electrostatic intermolecular interactions necessary for Cavin1 to function in caveola recruitment and sculpting.

Discussion

Despite the fact that intrinsically disordered sequences are a prominent and highly conserved feature of all cavins, there have been no previous studies that explicitly addressed their functional importance. We now show that they are essential for caveola formation. In addition, they also regulate the ability of Cavin1 to self-associate and undergo LLPS. *In vitro*, Cavin1 shows the classical properties of LLPS as demonstrated by phase separation that is sensitive to protein concentration, ionic strength, molecular crowding agents, and by the rapid exchange of protein in Cavin1 droplets as shown by FRAP. The sensitivity of this LLPS to salt concentration indicates an electrostatically driven Cavin1 condensation. We demonstrate the distinct roles of the disordered DR domains of Cavin1 in LLPS behaviour, including a mutant protein lacking the DR1 domain that still self-associates but no longer shows the dynamic exchange properties of the full-length protein. Our cellular studies show that acidic residues in all three Cavin1 disordered sequences (DR1, DR2 and DR3) are essential for generating caveolae with CAV1 at the plasma membrane. Deletion or mutation of these regions in Cavin1 result in mis-localisation and an inability to form plasma membrane caveola invaginations. Interestingly the N- and C-terminal sequences play divergent roles in this process. Deletion of the N-terminal DR1 domain leads to the formation of large intracellular clusters of Cavin1, CAV1, and endosomal membrane vesicles. In contrast, deletion of the DR3 domain prevents CAV1 association and results in dynamic microtubule association or cytoplasmic droplet formation. We speculate that Cavin1- Δ DR3 association with microtubules may share mechanistic similarities with the condensation of Tau on microtubules^{55,56}, or interactions of multivalent positively-charged peptides with the C-terminal acidic tails of tubulin subunits⁵⁷, but this will require further study.

To better appreciate and visualise the role of the disordered DR domains in Cavin1 activity, we constructed a theoretical structural model of the protein, building on the assumption that the fundamental Cavin1 unit is a homotrimer based on the coiled-coil structure of its N-terminal HR1 domain¹¹ (see Materials and Methods) (**Fig. 8A**). This model points to several interesting features of the Cavin1 protein. Firstly, the combined DR1, DR2 and DR3 domains account for more than 50% of the total Cavin1 sequence. In other words, Cavin1 is not a typical globular protein but rather consists of large random-coil elements tethered by α -helical structural cores. Secondly, as suggested by sequence analyses (**Fig. S1**), there is a distinctive electrostatic pattern to the structure, with the α -helical domains providing positively charged surfaces for membrane association, and the disordered regions having a generally negatively-charged nature. A likely consequence of this is that electrostatic repulsion will cause these DR domains will orient outwards when Cavin1 is in contact with membranes, and we propose they will also form transient electrostatic interactions with the HR domains of neighbouring Cavin1 molecules (**Fig. 8B**). Notably, it has been shown that

electrostatically-driven interactions between disordered proteins can lead to exceptionally high affinity complex formation under physiological conditions⁵⁸.

Our studies of the DR domains of Cavin1 confirm that the acidic residues within these domains are essential for the formation of caveolae in cells and promotion of membrane remodelling *in vitro*. By what mechanism might the DR domains contribute to these membrane sculpting activities? Several recent studies have demonstrated the ability of intrinsically disordered sequences to generate membrane curvature when coupled to membrane binding domains^{48, 59-61}. This is caused by molecular crowding of the disordered sequences leading the proteins to partition with curved or convex membranes so as to increase their conformational entropy; and this can also be enhanced by electrostatic repulsive forces between the disordered domains (**Fig. 8C**). One possible mechanism we can propose for Cavin1-driven membrane curvature is that negatively charged DR sequences and positively charged HR regions of Cavin1 combine to promote self-association, membrane interaction and protein crowding at the membrane surface leading to subsequent membrane bending. In the absence of CAV1 and at high protein concentrations *in vitro*, Cavin1 can generate arrays of protein oligomers to form membrane tubules. In mammalian cells however, the process of generating membrane curvature is tightly regulated by CAV1, EHD2 and Pacsin2, and also specific membrane lipids, to restrict Cavin1 remodelling activity only to caveolae. We see an almost complete correlation between the ability of different Cavin1 truncations and mutants to tubulate membranes *in vitro* and the ability to form caveolae *in situ*. The sole exception to this is Cavin1(1-345) mutant M4, where acidic residues in the DR3 region 310-345 are maintained but other side-chains are altered to alanine. This mutant is able to assemble into polymers and efficiently tubulate synthetic membranes, but forms cytoplasmic condensates and fails to generate caveolae in PC3 cells. This implies there are specific sequences in the Cavin1 DR3 region that are additionally required for Cavin1 recruitment to CAV1-positive membrane domains.

A second mechanism suggested by our results (and not mutually exclusive with a role for molecular crowding) is the formation of phase-separated Cavin1 domains at the membrane itself. Intrinsically disordered regions of proteins have gained significant attention for their ability to promote LLPS, or biomolecular condensation, with important biological functions such as stress granule formation, assembly of nuclear sub-structures and sensing changes in cellular homeostasis^{19, 62}. The plasma membrane and surfaces of intracellular compartments including the ER and lysosomes have been found to play a role in LLPS, acting as sites of droplet nucleation or as platforms for transport of phase-separated assemblies for example²³⁻³⁴. It has also recently been proposed that biomolecular condensates associated with phospholipid membranes might possess emergent mechanical properties that can result in membrane curvature generation³⁵⁻³⁷. This is depicted in schematic form in **Fig. 8D**. Here we have shown for the first time that purified Cavin1 can readily

undergo LLPS under near physiological conditions. The DR1 and DR3 domains contribute to this process, although neither domain is strictly essential. Indeed, mutations in DR3 that prevent CAV1 interaction at the plasma membrane promote GFP-Cavin1 liquid droplet formation in cells. Notably, removal of the DR1 domain results in apparent gel formation rather than liquid droplet assembly *in vitro*, and within cells results in a striking accumulation of large intracellular structures that also contain CAV1. These are formed by redistribution of caveola structures from the cell surface and accumulation with EEA1-positive endosomes. Caveolae, positive for both CAV1 and Cavin1, have been shown to bud from the plasma membrane and fuse with early endosomal compartments⁶³⁻⁶⁸, and this would almost certainly require dynamic remodelling of the protein coat to allow the process to occur. We postulate that the intracellular structures we observe with Cavin1-ΔDR1 are formed by internalised caveolae, which have become blocked during the stage of early endosomal fusion. This may be due to the DR1-truncated Cavin1 being unable to undergo normal dynamic exchange, as suggested by its gel-forming properties and its ability to cluster membrane vesicles *in vitro*, causing inhibition or slowing of the docking/fusion with the early endosome in a process involving EEA1 and Rab5a^{67,69}.

To conclude, our data indicates that the assembly of caveolae by Cavin1 strictly depends on a ‘fuzzy’ network of interactions promoted by electrostatic associations, with an essential role for the intrinsically disordered DR domains of Cavin1 in self-association, membrane remodelling and ultimately caveola formation. Fuzzy interactions are defined broadly as those that involve varying degrees of protein disorder or structural ambiguity; providing versatility and reversibility in protein-protein interactions⁷⁰⁻⁷². It has also been suggested that fuzzy interaction modes might be a driver of protein phase transitions¹⁹. This model for caveola assembly differs markedly from other classical membrane coats such as clathrin or COPI and COPII, which are built from symmetrical arrays of structured protein domain interactions. Although Cavin1 shows a capacity to form liquid droplets *in vitro* and in cells, we are cautious about asserting that LLPS by Cavin1 is strictly required for caveola formation⁷³. Alternatively, it may be that the LLPS behaviour of Cavin1 and its assembly at the membrane surface to generate curvature are due to related physicochemical and self-association processes. These studies clearly show, however, that the electrostatic properties of DR domains are required for Cavin1 to function in caveola formation and trafficking.

Materials and methods

Cell lines maintenance and materials

PC3 cells were maintained in RPMI medium (Gibco® Life technologies) supplemented with 10% fetal bovine serum (FBS) and Penicillin/Streptomycin. Cell lines were sourced from ATCC and tested fortnightly for mycoplasma contamination. For all experiments, 2×10^5 PC3 or MCF7 cells were plated in either 6 well culture dishes (Nunc™, Cat. No. 140675, Culture area - 9.6 cm²) or glass bottom 35 mm dishes (ibidi, No. 1.5 glass coverslip bottom Cat No. 81218) or 35mm tissue culture dishes (TPP® 93040, culture area - 9.2 cm²). Antibodies used were as follows, rabbit polyclonal anti-Caveolin1 (BD Transduction Laboratories, Cat. No. 610060), mouse monoclonal anti-GFP (Roche Diagnostics Cat. No. 11814460001), Donkey anti-Rabbit IgG (H+L) Secondary Antibody Alexa Fluor® 555 conjugate (Thermo Fisher Scientific, Cat No. A31572). Mouse monoclonal anti-tubulin (Anti-alpha Tubulin antibody [DM1A] - Abcam (ab7291)). Folch lipids were obtained from Sigma Aldrich Folch I fraction (B1502)

Molecular cloning and plasmids

For Recombinant protein expression in *E. coli* two vectors (pHUE and pOPINE-GFP) were used to generate Cavin1 DR domain variants summarised in **Fig. S1**. pHUE vector was used to generate N-terminal 6X-Histidine-Ubiquitin tagged DR domain variants of Cavin1 using overlap extension polymerase chain reaction (OE-PCR) technique at SacII restriction enzyme site⁷⁴. GFP tagged cavin DR domain variants were generated using pOPINE-GFP vector (in house vector with pOPINE backbone containing GFP) BamHI restriction enzyme site with N-terminal 6X-Histidine-Ubiquitin tag and C-terminal GFP tag using OE-PCR⁷⁵. For mammalian cell expression constructs, eGFPC1 and eGFPN1 vectors were used to generate respective DR domain Cavin1 mutants summarised in **Fig. S2**. Specific Cavin1 (1-345) DR domain genes (summarised in **Fig. 7A**) were artificially synthesized (Gene Universal) and subsequently cloned into eGFPC1, pHUE vector using OE-PCR.

Recombinant protein expression and purification

Recombinant protein expression was performed using *Escherichia coli* strain Rosetta™ 2 (DE3) (Novagen) (Merck Cat. No 71403). Protein expression was always performed using freshly transformed chemically competent *E. coli* Rosetta 2 cells with respective plasmids. Cell were propagated in either LB or TB media and protein expression was performed by inducing with 0.5 mM IPTG (Isopropyl β-D-1-thiogalactopyranoside, Bioline, Cat No. BIO-37036) overnight at 18°C. Next day, cells were harvested in 20 mM HepesKOH (pH 7.6), 500 mM NaCl (500GF buffer) with addition of benzamidine hydrochloride (Sigma Aldrich, B6506) and cOmplete™, EDTA-free

Protease Inhibitor Cocktail Roche (Sigma Aldrich, 4693132001). Cleared cell lysates were prepared using a continuous flow cell disruptor (Constant Systems Limited, UK) at pressure range 25 – 30 kPsi with subsequent addition of 0.5 % w/v Triton X-100 and 5 mM imidazole (Sigma Aldrich, 792527) followed by centrifugation 35,000x g for 30 min. Purification of 6X-Histidine tagged cavin proteins was done using TALON metal affinity resin (ClonTech, Scientifix Cat No. 635503). Talon resin was thoroughly washed with 500GF buffer containing 5 mM imidazole to remove detergent and non-specifically bound proteins, and elution was performed in 500GF buffer containing 300 mM imidazole. Protein samples were immediately loaded on size exclusion chromatography column Superose 6 10/30GL pre-equilibrated with 20 mM HepesKOH pH7.6, 150 mM NaCl (150GF buffer). Size exclusion profiles of purified cavin truncation mutants are shown in **Fig. S6**. The purified protein used in assays (marked with arrows) appears to be slightly truncated but forms part of megadalton size full length protein complex eluting in higher molecular weight fractions (**Fig. S6**). This partial truncation can be due to presence of multiple protease sensitive PEST (proline, glutamate, serine, threonine) regions in DR sequences of Cavin1⁹. There has been evidence for the presence of truncated species of Cavin1 bound to native caveolae in cells suggesting that this might be an inherent property of this protein regardless of its source of expression^{7, 76}.

Fluorescence correlation spectroscopy (FCS) analysis

FCS analysis was performed on a Zeiss LSM 710 confocal microscope equipped with 40x/1.2W C-Apo lens and twin BiG GaAsP detectors capable of single molecule detection. Briefly, MCF7 cells were lysed in a buffer (200 μ l) containing 25 mM Tris (pH 7.4), 150 mM NaCl while passing through a 27G needle 6 times. Lysates were then centrifuged at 17,000x g for 10 min to remove cell debris. Supernatant was then used for FCS analysis. Purified GFP tagged cavin proteins were prepared for FCS by dilution of respective stock solutions of cavin truncates in either 500GF or 150GF buffer to achieve 0.1 μ M protein concentration with subsequent centrifugation at 17,000 X g for 10 min. At the beginning of each FCS session on a Zeiss LSM 710, pinhole calibration was done with BODIPY-FL maleimide dye (Cat. No. B30466). Subsequently, diffusion time for three dyes that differ in molecular weight and particle size BODIPY-FL maleimide (~24 μ s), BODIPY-FL iodoacetamide (~22 μ s) and TAMRA DIBO (~37 μ s) was measured for each session (**Fig. S7I**). FCS measurement for each GFP tagged Cavin protein was then done for 10 s and repeated 10 times with a binning time of 200 ns. FCS measurements showing presence of aggregates were removed from analysis. The autocorrelation function $G(\tau)$ was fitted using a predefined isotropic 3D translational diffusion $G_d(\tau)$ model from the ConFoCor model tool with fixed amplitude (A) and structural parameter, $G(\tau) = 1 + A * G_d(\tau)$. The diffusion coefficient or diffusivity (μ s²Sec⁻¹) for each measurement was exported from the Zeiss analysis program and plotted for all constructs in Graph pad Prism software. Hydrodynamic

radius calculations were done using Stokes-Einstein equation with basic assumption of perfect spherical object diffusion. Stokes – Einstein equation; $D = K_B T / 6\pi n r$, Where, K_B – Boltzmann constant, T – Temperature (298K), π – pi (3.14), n – dynamic viscosity (Pa.S) and r – hydrodynamic (Stokes) radius of spherical particle.

In vitro phase separation assays

Purified GFP tagged Cavin1 proteins were diluted to respective protein and/or salt concentrations prior to addition of dextran T-500 (Pharmacia). Dextran solution was added on the top of protein solution without any mixing to allow natural diffusion of dextran. Image acquisition and fluorescence recovery after photobleaching (FRAP) assays were performed after 2 min wait period to allow phase separated droplets to settle. Phase separation analysis was done within 10 min post addition of dextran. Non-bleaching image acquisition conditions were established before performing FRAP assay. FRAP analysis was done by bleaching rectangular area (2 μm X 1 μm approximately) within protein droplet using 488 nm Argon laser and subsequent image acquisition was done one frame per second. Recovery curves from different proteins were normalised without acquisition bleaching correction using formula $[F_{(T)} - F_{(\text{postbleach}T=0)}] / [F_{(\text{Prebleach})} - F_{(\text{postbleach}T=0)}]$. Normalised data points were used to perform non-linear exponential recovery fit using equations within ImageJ 1.50g or Prism version 8 to obtain half-life value for fluorescence recovery of respective protein.

Liposome preparation and in vitro membrane tubulation assay

Liposomes were prepared by mixing of 10 μL 10 mM stock solution of Folch lipids (bovine brain extract lipid - Folch I fraction Sigma Aldrich B1502) with 50 μL chloroform in a round-bottom flask. The mixtures were dried gently by a stream of nitrogen first and under vacuum overnight thereafter. Liposomes were rehydrated in 500 μL 150GF buffer followed by repetitive freeze-thaw cycles for 3 – 5 times, using first a mixture of dry ice and acetone followed with 60°C water. The liposomes were then extruded through a 400-nm polycarbonate membrane 21 times using an Avanti mini-extruder to generate large unilamellar lipid vesicles (LUVs).

A 5 μl volume of purified Cavin1 variants [\sim 0.1 mg/ml (1.5 – 2 μM)] was mixed with 5 μl 200 μM liposomes for 1 – 3 min at room temperature. Samples were then quickly spotted onto formvar-carbon coated electron microscopy grids (Cu/Pd grids 200 mesh hexagonal – ProSciTech - GCU-PD200H) for 10 s and excess samples were removed by blotting at corner using Whatman filter paper. This is followed by 2 - 3 distilled water washes in similar fashion and subsequent application of 1% uranyl acetate stain. The excess of stain was removed by blotting and grids were allowed to air

dry for a while before viewing under the electron microscope. Final images were acquired on JEOL 1011 electron microscope at 80 kV.

Giant multilamellar vesicle (GMV) experiments

Giant multilamellar vesicles (GMV) were prepared using electro-formation method described before⁷⁷. Briefly, lipids mixture dissolved in chloroform / methanol solution was gently applied to indium-tin-oxide coated glass slide (Sigma Aldrich Cat. No. 636908) as multiple layers. This solution was then dried under constant stream of nitrogen to remove organic solvent and further dried under vacuum overnight. Next day, electro-formation was performed at 50⁰C in 150GF buffer for 1 hr. Vesicles were used immediately for experiments.

Cryoelectron microscopy / tomography of Cavin1 coated membrane tubules

Liposome tubulation reaction was assembled as described in the previous section and subjected to vitrification after a 1 – 3 min incubation period. For vitrification, the sample was applied to Lacey carbon grids (EMS, Hatfield, PA, USA) using a Vitrobot Mark II (FEI, Eindhoven, NL) plunge freezer with 4 μ l of sample, 6 s blotting time and a -3 mm offset at 24⁰C and 100% humidity. Images were collected on a Tecnai G2 F30 TEM (FEI, Eindhoven, NL) operated at 300 kV at a magnification of 12,000X with 5 μ m defocus. Images were recorded on a Gatan K2 summit camera in counting mode for a final pixel size of 3.556 Å per pixel. Images were processed in either IMOD (version 4.9) or ImageJ.

Tilt-series were acquired on a Talos Arctica TEM (Thermo Fisher Scientific-FEI, Eindhoven, NL) operated at 200 kV and at a magnification of 45,000x (final pixel size 3.11 Å per pixel). Images were recorded using the microscope software Tomography (Thermo Fisher Scientific-FEI, NL) on Falcon 3 (Thermo Fisher Scientific-FEI, NL) camera operated in counting mode at an angular range of -60⁰ to 60⁰ in a bidirectional fashion and at an angular increment of 2⁰. The defocus was set to -5 μ m. Unbinned movies of 8 frames with a set dose rate of ~ 1.7 e/Å² were acquired and tomographic reconstructions were generated using the weighted back-projection method in IMOD (<https://bio3d.colorado.edu/imod/> version 4.9).

Electron microscopy processing of PC3 cells

PC3 cells were plated onto 30 mm tissue culture dishes and allowed to adhere to dishes for 48 h prior to transfection. Cells were then co-transfected with APEX-GBP and respective cavin1 mutant constructs. 24 h post transfection, cells were fixed with 2.5% glutaraldehyde in 0.1 M sodium cacodylate buffer (cacodylate) (pH7.4) for 1 h. DAB (3,3'-diaminobenzidine tetrahydrochloride, Sigma-Aldrich Cat. No. D5905) reaction was then performed as follows. Briefly, cells were washed

with DAB/cacodylate mixture (DAB final concentration – 1 mg/ml) for 2 mins, then treated with DAB/cacodylate + 5.88 mM H₂O₂ (hydrogen peroxide, Sigma-Aldrich Cat. No. H1009) for 20 mins. Cells were then washed with 0.1 M sodium cacodylate buffer and contrasted with 1% osmium tetroxide for 2 mins. Cells were then embedded in LX112 resin and thin sections were cut as described previously⁵². Images were acquired on JEOL 1011 electron microscope fitted with a Morada CCD camera (Olympus) under the control of iTEM software and operated at 80kV.

Immunofluorescence analysis, live cell imaging and Proximity ligation assay (PLA)

PC3 cells were grown at about ~50% confluency in RPMI 1640 medium supplemented with 10% FBS. Cells were then transfected with respective Cavin1 mutants using Lipofectamine 3000 (Invitrogen) as per manufacturer's instructions. Cells were fixed 24 h post transfection with 4% paraformaldehyde in phosphate-buffered saline (PBS) at 4°C and subsequently permeabilised with 0.1% Triton X-100 in PBS for 7 mins. Cells were probed with CAV1 antibody (Dilution 1:600) and anti-Rabbit secondary antibody Alexa Fluor® 561 conjugate (Dilution 1:400). Confocal images (1024X1024) were acquired on Zeiss inverted LSM 880 coupled with fast airyscan detector (Carl Zeiss, Inc) equipped with 63X oil immersion objective, NA 1.4. Images were acquired at different laser power for GFP tagged truncation mutants and detector gain settings in order to avoid oversaturation of pixels. All images were processed for brightness/contrast (histogram) adjustment for visualisation using ImageJ. For live cell imaging and FRAP analysis, cells were plated on glass bottom (No. 1.5) petri dishes (ibidi) and allowed to grown at about ~70% confluency and transfected with respective Cavin1 mutants. For bleaching, 488 nm laser at 100% attenuation power was used for 20 iterations and subsequent imaging was done at one frame per second. Airyscan processing was done automatically in Zeiss software (ZEN 2.3). For PLA, PC3 cells were processed as described previously¹⁰. Images were then acquired on Zeiss LSM 710 and LSM 880 confocal microscope (Carl Zeiss, Inc) equipped with 63X oil immersion objective and quantitation of PLA dots per cell was performed using find maxima function in ImageJ with offset of 25.

Constructing a structural model of mouse Cavin1

A structural model of mouse Cavin1 was built manually based both known structures of the mouse Cavin1 HR1 domain¹¹ (PDB ID 4QKV), the previous model of the Cavin1 undecad UC1 region¹⁰, and secondary structure prediction of the Cavin1 protein carefully cross-referenced to several Cavin1 homologues and other Cavin family members¹¹. Based on the homotrimeric coiled-coil structure of the HR1 domain we constructed our model under the assumption that a single Cavin1 'unit' would consist of three identical Cavin1 chains. The secondary structure predictions and previous crystal

structure led us to define the following regions of Cavin1 as either α -helical or random-coil; DR1, residues 1-48, random-coil; HR1, residues 49-147, α -helical (based on PDB 4QKV of mouse Cavin1 HR1); DR2, residues 148-218, random-coil; HR2, α -helical for residues 219-242, random-coil for residues 243-244, α -helical for residues 245-278 (model from ¹⁰), random-coil for residues 279-286, α -helical for residues 287-297; DR3, residues 298-392, random coil. Stretches of random-coil were built and added to α -helical domains manually in COOT Version 0.8.2 ⁷⁸, and the final model was subjected to simple geometry regularisation in PHENIX Version 1.14 ⁷⁹. Structural images and electrostatic surface representations were rendered with PYMOL Version 2.3.1.

Statistical analyses

Statistical analysis and P value calculations were performed by one-way ANOVA using graph pad Prism software.

Acknowledgements

This work was supported by grants from the National Health and Medical Research Council of Australia (NHMRC) (to RGP grant number APP569542 and APP1037320) and the Australian Research Council (ARC) (to BMC, grant number DP120101298). RGP is supported by an NHMRC Senior Principal Research Fellowship from the NHMRC (APP1058565) and by the Australian Research Council Centre of Excellence in Convergent Bio-Nano Science and Technology (R.G. Parton). BMC is supported by an NHMRC Senior Research Fellowship (APP1136021). Confocal microscopy was performed at the Australian Cancer Research Foundation (ACRF)/Institute for Molecular Bioscience (IMB) Dynamic Imaging Facility for Cancer Biology, established with funding from the ACRF. The authors acknowledge the Victor Chang Innovation Centre, funded by the NSW Government, and facilities at the Electron Microscope Unit within the Mark Wainwright Analytical Centre at UNSW Sydney.

Author contributions

BMC and RGP conceived the project, study and acquired funding. VT performed molecular cloning, in vitro protein purification, in vitro, cellular assays, live imaging and FCS experiments. GY assisted in molecular cloning and in vitro protein purification. KA assisted in cellular and phase separation assay. JR performed cellular processing for electron microscopy and image acquisition. NA and MF performed tomography data acquisition, and trained VT in cryo-EM methods. All authors commented on the manuscript. VT, RGP and BMC wrote the manuscript.

Conflict of interest

Authors declare that they have no conflict of interest.

References

1. Lamaze, C., Tardif, N., Dewulf, M., Vassilopoulos, S. & Blouin, C.M. The caveolae dress code: structure and signaling. *Current Opinion in Cell Biology* **47**, 117-125 (2017).
2. Parton, R.G. & del Pozo, M.A. Caveolae as plasma membrane sensors, protectors and organizers. *Nature reviews. Molecular cell biology* **14**, 98-112 (2013).
3. Parton, R.G. Caveolae: Structure, Function, and Relationship to Disease. *Annual Review of Cell and Developmental Biology* **34**, 111-136 (2018).
4. Hayer, A., Stoeber, M., Bissig, C. & Helenius, A. Biogenesis of caveolae: stepwise assembly of large caveolin and cavin complexes. *Traffic* **11**, 361-382 (2010).
5. Ariotti, N. *et al.* Molecular Characterization of Caveolin-induced Membrane Curvature. *The Journal of biological chemistry* **290**, 24875-24890 (2015).
6. Busija, A.R., Patel, H.H. & Insel, P.A. Caveolins and cavins in the trafficking, maturation, and degradation of caveolae: implications for cell physiology. *Am J Physiol Cell Physiol* **312**, C459-C477 (2017).
7. Hill, M.M. *et al.* PTRF-Cavin, a conserved cytoplasmic protein required for caveola formation and function. *Cell* **132**, 113-124 (2008).
8. Walser, P.J. *et al.* Constitutive formation of caveolae in a bacterium. *Cell* **150**, 752-763 (2012).
9. Bastiani, M. *et al.* MURC/Cavin-4 and cavin family members form tissue-specific caveolar complexes. *The Journal of cell biology* **185**, 1259-1273 (2009).
10. Tillu, V.A. *et al.* A variable undecad repeat domain in cavin1 regulates caveola formation and stability. *EMBO reports* **19**, e45775 (2018).
11. Kovtun, O. *et al.* Structural insights into the organization of the cavin membrane coat complex. *Developmental cell* **31**, 405-419 (2014).
12. Kovtun, O., Tillu, V.A., Ariotti, N., Parton, R.G. & Collins, B.M. Cavin family proteins and the assembly of caveolae. *Journal of cell science* **128**, 1269-1278 (2015).
13. Mohan, J., Moren, B., Larsson, E., Holst, M. & Lundmark, R. Cavin3 interacts with cavin1 and caveolin1 to increase surface dynamics of caveolae. *Journal of cell science* (2015).
14. Gambin, Y. *et al.* Single-molecule analysis reveals self assembly and nanoscale segregation of two distinct cavin subcomplexes on caveolae. *eLife* **3**, e01434 (2014).
15. Oates, M.E. *et al.* D2P2: database of disordered protein predictions. *Nucleic Acids Research* **41**, D508-D516 (2012).
16. Banks, D.S. & Fradin, C. Anomalous diffusion of proteins due to molecular crowding. *Biophys J* **89**, 2960-2971 (2005).

17. Lavie, Y., Fiucci, G. & Liscovitch, M. Up-regulation of caveolae and caveolar constituents in multidrug-resistant cancer cells. *The Journal of biological chemistry* **273**, 32380-32383 (1998).
18. Tillu, V.A., Kovtun, O., McMahon, K.A., Collins, B.M. & Parton, R.G. A phosphoinositide-binding cluster in cavin1 acts as a molecular sensor for cavin1 degradation. *Mol Biol Cell* **26**, 3561-3569 (2015).
19. Boeynaems, S. *et al.* Protein Phase Separation: A New Phase in Cell Biology. *Trends Cell Biol* **28**, 420-435 (2018).
20. Boyko, S., Qi, X., Chen, T.H., Surewicz, K. & Surewicz, W.K. Liquid-liquid phase separation of tau protein: The crucial role of electrostatic interactions. *The Journal of biological chemistry* **294**, 11054-11059 (2019).
21. Gomes, E. & Shorter, J. The molecular language of membraneless organelles. *The Journal of biological chemistry* **294**, 7115-7127 (2019).
22. Wang, J. *et al.* A Molecular Grammar Governing the Driving Forces for Phase Separation of Prion-like RNA Binding Proteins. *Cell* **174**, 688-699 e616 (2018).
23. Alenquer, M. *et al.* Influenza A virus ribonucleoproteins form liquid organelles at endoplasmic reticulum exit sites. *Nat Commun* **10**, 1629 (2019).
24. Case, L.B., Zhang, X., Ditlev, J.A. & Rosen, M.K. Stoichiometry controls activity of phase-separated clusters of actin signaling proteins. *Science* **363**, 1093-1097 (2019).
25. Ditlev, J.A. *et al.* A composition-dependent molecular clutch between T cell signaling condensates and actin. *eLife* **8** (2019).
26. Huang, W.Y.C. *et al.* A molecular assembly phase transition and kinetic proofreading modulate Ras activation by SOS. *Science* **363**, 1098-1103 (2019).
27. Johnson, A. *et al.* TFG clusters COPII-coated transport carriers and promotes early secretory pathway organization. *EMBO J* **34**, 811-827 (2015).
28. Liao, Y.C. *et al.* RNA Granules Hitchhike on Lysosomes for Long-Distance Transport, Using Annexin A11 as a Molecular Tether. *Cell* **179**, 147-164 e120 (2019).
29. Ma, W. & Mayr, C. A Membraneless Organelle Associated with the Endoplasmic Reticulum Enables 3'UTR-Mediated Protein-Protein Interactions. *Cell* **175**, 1492-1506 e1419 (2018).
30. Milovanovic, D., Wu, Y., Bian, X. & De Camilli, P. A liquid phase of synapsin and lipid vesicles. *Science* **361**, 604-607 (2018).
31. Snead, W.T. & Gladfelter, A.S. The Control Centers of Biomolecular Phase Separation: How Membrane Surfaces, PTMs, and Active Processes Regulate Condensation. *Mol Cell* **76**, 295-305 (2019).
32. Zappa, F. *et al.* The TRAPP complex mediates secretion arrest induced by stress granule assembly. *EMBO J* **38**, e101704 (2019).

33. Beutel, O., Maraspini, R., Pombo-García, K., Martin-Lemaitre, C. & Honigsmann, A. Phase Separation of Zonula Occludens Proteins Drives Formation of Tight Junctions. *Cell* **179**, 923-936.e911 (2019).
34. Schwayer, C. *et al.* Mechanosensation of Tight Junctions Depends on ZO-1 Phase Separation and Flow. *Cell* **179**, 937-952.e918 (2019).
35. Bergeron-Sandoval, L.P. & Michnick, S.W. Mechanics, Structure and Function of Biopolymer Condensates. *J Mol Biol* **430**, 4754-4761 (2018).
36. Lacy, M.M., Ma, R., Ravindra, N.G. & Berro, J. Molecular mechanisms of force production in clathrin-mediated endocytosis. *FEBS Lett* **592**, 3586-3605 (2018).
37. Bergeron-Sandoval, L.-P. *et al.* Endocytosis caused by liquid-liquid phase separation of proteins. *bioRxiv* **145664** (2017).
38. Li, Y., Lipowsky, R. & Dimova, R. Membrane nanotubes induced by aqueous phase separation and stabilized by spontaneous curvature. *Proc Natl Acad Sci U S A* **108**, 4731-4736 (2011).
39. Alberti, S. *et al.* A User's Guide for Phase Separation Assays with Purified Proteins. *J Mol Biol* **430**, 4806-4820 (2018).
40. Wang, Z., Zhang, G. & Zhang, H. Protocol for analyzing protein liquid-liquid phase separation. *Biophysics Reports* **5**, 1-9 (2019).
41. Molliex, A. *et al.* Phase separation by low complexity domains promotes stress granule assembly and drives pathological fibrillization. *Cell* **163**, 123-133 (2015).
42. Alberti, S., Gladfelter, A. & Mittag, T. Considerations and Challenges in Studying Liquid-Liquid Phase Separation and Biomolecular Condensates. *Cell* **176**, 419-434 (2019).
43. Rothberg, K.G. *et al.* Caveolin, a protein component of caveolae membrane coats. *Cell* **68**, 673-682 (1992).
44. Shaul, P.W. & Anderson, R.G. Role of plasmalemmal caveolae in signal transduction. *Am J Physiol* **275**, L843-851 (1998).
45. Ludwig, A. *et al.* Molecular composition and ultrastructure of the caveolar coat complex. *PLoS Biol* **11**, e1001640 (2013).
46. Ludwig, A., Nichols, B.J. & Sandin, S. Architecture of the caveolar coat complex. *Journal of cell science* **129**, 3077-3083 (2016).
47. Stoeber, M. *et al.* Model for the architecture of caveolae based on a flexible, net-like assembly of Cavin1 and Caveolin discs. *Proc Natl Acad Sci U S A* **113**, E8069-E8078 (2016).
48. Snead, W.T. *et al.* BAR scaffolds drive membrane fission by crowding disordered domains. *The Journal of cell biology* **218**, 664-682 (2019).
49. Wang, S., Zhao, Z. & Rodal, A.A. Higher-order assembly of Sorting Nexin 16 controls tubulation and distribution of neuronal endosomes. *The Journal of cell biology* **218**, 2600 (2019).

50. Khater, I.M., Meng, F., Wong, T.H., Nabi, I.R. & Hamarneh, G. Super Resolution Network Analysis Defines the Molecular Architecture of Caveolae and Caveolin-1 Scaffolds. *Scientific Reports* **8**, 9009 (2018).
51. Liu, L. & Pilch, P.F. A critical role of cavin (polymerase I and transcript release factor) in caveolae formation and organization. *The Journal of biological chemistry* **283**, 4314-4322 (2008).
52. Ariotti, N. *et al.* Modular Detection of GFP-Labeled Proteins for Rapid Screening by Electron Microscopy in Cells and Organisms. *Developmental cell* **35**, 513-525 (2015).
53. Hetmanski, J.H.R. *et al.* Membrane Tension Orchestrates Rear Retraction in Matrix-Directed Cell Migration. *Developmental cell* (2019).
54. Pelkmans, L. & Zerial, M. Kinase-regulated quantal assemblies and kiss-and-run recycling of caveolae. *Nature* **436**, 128 (2005).
55. Siahaan, V. *et al.* Kinetically distinct phases of tau on microtubules regulate kinesin motors and severing enzymes. *Nat Cell Biol* **21**, 1086-1092 (2019).
56. Tan, R. *et al.* Microtubules gate tau condensation to spatially regulate microtubule functions. *Nat Cell Biol* **21**, 1078-1085 (2019).
57. Drechsler, H., Xu, Y., Geyer, V.F., Zhang, Y. & Diez, S. Multivalent electrostatic microtubule-interactions of synthetic peptides are sufficient to mimic advanced MAP-like behaviour. *Mol Biol Cell*, mbcE19050247 (2019).
58. Borgia, A. *et al.* Extreme disorder in an ultrahigh-affinity protein complex. *Nature* **555**, 61-66 (2018).
59. Zeno, W.F. *et al.* Synergy between intrinsically disordered domains and structured proteins amplifies membrane curvature sensing. *Nat Commun* **9**, 4152 (2018).
60. Zeno, W.F. *et al.* Molecular Mechanisms of Membrane Curvature Sensing by a Disordered Protein. *J Am Chem Soc* **141**, 10361-10371 (2019).
61. Busch, D.J. *et al.* Intrinsically disordered proteins drive membrane curvature. *Nature Communications* **6**, 7875 (2015).
62. Yoo, H., Triandafillou, C. & Drummond, D.A. Cellular sensing by phase separation: Using the process, not just the products. *The Journal of biological chemistry* **294**, 7151-7159 (2019).
63. Aoki, T., Hagiwara, H., Matsuzaki, T., Suzuki, T. & Takata, K. Internalization of caveolae and their relationship with endosomes in cultured human and mouse endothelial cells. *Anat Sci Int* **82**, 82-97 (2007).
64. Boucrot, E., Howes, M.T., Kirchhausen, T. & Parton, R.G. Redistribution of caveolae during mitosis. *Journal of cell science* **124**, 1965-1972 (2011).
65. Hayer, A. *et al.* Caveolin-1 is ubiquitinated and targeted to intraluminal vesicles in endolysosomes for degradation. *The Journal of cell biology* **191**, 615-629 (2010).
66. Jung, W. *et al.* Cell-free formation and interactome analysis of caveolae. *The Journal of cell biology* **217**, 2141-2165 (2018).

67. Pelkmans, L., Burli, T., Zerial, M. & Helenius, A. Caveolin-stabilized membrane domains as multifunctional transport and sorting devices in endocytic membrane traffic. *Cell* **118**, 767-780 (2004).
68. Shvets, E., Bitsikas, V., Howard, G., Hansen, C.G. & Nichols, B.J. Dynamic caveolae exclude bulk membrane proteins and are required for sorting of excess glycosphingolipids. *Nat Commun* **6**, 6867 (2015).
69. Murray, D.H. *et al.* An endosomal tether undergoes an entropic collapse to bring vesicles together. *Nature* **537**, 107-111 (2016).
70. Miskei, M. *et al.* Fuzziness enables context dependence of protein interactions. *FEBS Lett* **591**, 2682-2695 (2017).
71. Olsen, J.G., Teilum, K. & Kragelund, B.B. Behaviour of intrinsically disordered proteins in protein-protein complexes with an emphasis on fuzziness. *Cell Mol Life Sci* **74**, 3175-3183 (2017).
72. Tompa, P. & Fuxreiter, M. Fuzzy complexes: polymorphism and structural disorder in protein-protein interactions. *Trends Biochem Sci* **33**, 2-8 (2008).
73. McSwiggen, D.T., Mir, M., Darzacq, X. & Tjian, R. Evaluating phase separation in live cells: diagnosis, caveats, and functional consequences. *Genes Dev* (2019).
74. Catanzariti, A.M., Soboleva, T.A., Jans, D.A., Board, P.G. & Baker, R.T. An efficient system for high - level expression and easy purification of authentic recombinant proteins. *Protein Science* **13**, 1331-1339 (2004).
75. Berrow, N.S. *et al.* A versatile ligation-independent cloning method suitable for high-throughput expression screening applications. *Nucleic Acids Research* **35**, e45-e45 (2007).
76. Aboulaich, N., Vainonen, J.P., Stralfors, P. & Vener, A.V. Vectorial proteomics reveal targeting, phosphorylation and specific fragmentation of polymerase I and transcript release factor (PTRF) at the surface of caveolae in human adipocytes. *The Biochemical journal* **383**, 237-248 (2004).
77. Angelova, M.I. & Dimitrov, D.S. Liposome electroformation. *Faraday Discussions of the Chemical Society* **81**, 303-311 (1986).
78. Emsley, P. & Cowtan, K. Coot: model-building tools for molecular graphics. *Acta Crystallogr D Biol Crystallogr* **60**, 2126-2132 (2004).
79. Adams, P.D. *et al.* PHENIX: a comprehensive Python-based system for macromolecular structure solution. *Acta Crystallogr D Biol Crystallogr* **66**, 213-221 (2010).

Figure Legends

Figure 1. The Cavin1 N- and C-terminal DR domains are important for self-association into polymers.

(A) Schematic representation of Cavin1 and truncations. DR, disordered region; HR, helical region. (B) The diffusion rate of Cavin1, Cavin1- Δ DR1 and Cavin1- Δ DR3 in solution assessed by fluorescence correlation spectroscopy (FCS). Bacterially expressed and purified ubiquitin and GFP tagged proteins (Fig. S2) were analysed in high NaCl concentration (500 mM) and physiological NaCl concentration (150 mM). Error bars indicate mean \pm SD (standard deviation), N=2, n=10-15, ns – not significant, *P<0.05 ***P<0.001. (C) The diffusion rate of GFP-tagged Cavin1, Cavin1- Δ DR1 and Cavin1- Δ DR3 in lysates after expression in MCF7 cells (lacking endogenous Cavins and Caveolins). Buffer contained 150 mM NaCl. N=3, n=20-25, ns – not significant, ***P<0.001. Error bars indicate mean \pm SD.

Figure 2. Cavin1 undergoes liquid-liquid phase separation *in vitro*.

(A) Liquid-liquid phase separation (LLPS) assays with recombinant Ub- and GFP-tagged Cavin1, Cavin1- Δ DR3 and Cavin1- Δ DR1 at different protein and salt concentrations. (B) Fluorescence recovery after photobleaching (FRAP) assay with Cavin1, Cavin1- Δ DR3 and Cavin1- Δ DR1 showing GFP fluorescence images at increasing times. (C) Plot of normalized fluorescence intensity after photobleaching. N=6-8, Grey, blue and pink shaded areas around recovery curves represent standard deviation (SD). While Cavin1 and Cavin1- Δ DR3 droplets rapidly exchange with the bulk solution and recover their fluorescence, Cavin1- Δ DR1 shows virtually no exchange indicating gel formation.

Figure 3. The Cavin1 DR domains are required for membrane remodelling *in vitro*.

(A) Purified Ub-tagged full length Cavin1 was mixed with Folch 400 nm unilamellar liposomes and analysed by both negative stain EM (1% uranyl acetate) and cryoEM. (B) Cryoelectron tomography (CryoET) of Cavin1-coated membrane tubules showing bottom, middle and top sections of three-dimensional projections. Striated protein densities are observed coating the relatively heterogeneous membrane tubules. The full tomogram is shown in Movie S1. (C) Schematic diagram of Cavin1 and different truncation constructs examined for their ability to remodel membranes *in vitro*. (D) Purified Ub-tagged Cavin1 truncations were mixed with Folch 400 nm unilamellar liposomes and analysed by negative stain EM (1% uranyl acetate). Full membrane tubulation and remodelling activity requires residues 1-30 in DR1, and residues 330-345 in DR3.

Figure 4. Removing the Cavin1 DR domains prevents deformation of GUV membranes.

(A) Purified Ub- and GFP-tagged Cavin1 shows strong localised clustering on the surface of Folch giant multilamellar vesicles (GMV) containing Bodipy-TMR-labelled PI(4,5)P₂ (0.1 mol%). Cavin1 (B), Cavin1-ΔDR3 (C) or Cavin1-ΔDR1 (D) were incubated with Folch GMVs containing Bodipy-TMR-labelled PI(4,5)P₂ (0.1 mol%), allowed to settle on glass coverslips and images were acquired one frame per second. (E) GUVs incubated with Cavin1-ΔDR1 were often observed to be tethered to each other with Cavin1-ΔDR1 concentrated at the contact sites.

Figure 5. The Cavin1 DR domains are essential for caveola formation with CAV1.

(A) GFP-tagged Cavin1 and truncations (green) were expressed for 24 h in PC3 cells, fixed and immunolabelled for Caveolin1 (CAV1) (red). Full length Cavin1 forms typical caveola puncta, colocalising with CAV1 at the cell surface. Cavin1-ΔDR1 mutant expression leads to formation of tethered intracellular CAV1-positive clusters. Cavin1-ΔDR3 shows cytoplasmic and microtubule localisation. Images were collected using a Zeiss fast Airyscan microscope. Fluorescence recovery after photobleaching (FRAP) analysis of GFP-Cavin1-ΔDR3 before (B) and after (C) nocodazole (10 μM) addition. (D) In PC3 cells GFP-tagged Cavin1-ΔDR1 truncation shows colocalization with the early endosomal marker (EEA1) (red) and CAV1 (blue). Inset shows merge images of GFP-Cavin1-ΔDR1/EEA1 and GFP-Cavin1-ΔDR1/CAV1. (E) GFP-tagged Cavin1 and Cavin1-ΔDR1 were visualised in PC3 cells by electron microscopy and labelling of GFP tagged proteins using APEX-GBP staining. (F) Live imaging of PC3 cells expressing Rab5a-mCherry with either GFP-Cavin1 or GFP-Cavin1-ΔDR1. Images were acquired one frame per four seconds and frame numbers are indicated in boxes. Arrows indicate mCherry/GFP signal co-localisation or separation event.

Figure 6. Definition of the minimal DR sequences required for Cavin1 function.

(A) GFP-tagged Cavin1 DR domain truncation mutants (green) (Fig. 3C) were expressed in PC3 cells and immunolabelled with CAV1 (red). Residues 1-30 in DR1 and 330-345 are required for caveola formation. (B) APEX-GBP labelling of GFP tagged Cavin1(1-345) shows normal bulb-shaped caveolae at the plasma membrane. (C) Proximity ligation assay (PLA) analyses show that truncation of Cavin1 from the C-terminus beyond residue 345 results in loss of association with CAV1. PLA signal was quantified as dots per cell for specific interaction between GFP-tagged proteins and CAV1, N = 2 (independent biological replicates), n = 10-15 (cells per replicates), Error bars indicate mean ± SD, *** P<0.001.

Figure 7. DR-dependent Cavin1 higher order polymer formation and caveola assembly.

(A) Schematic diagram of Cavin1(1-345) with the sequences of the M1-M5 point mutants indicated. M1 substitutes all Asp/Glu residues for Ala in the DR1 region 1 to 30. M2 substitutes all residues apart from Asp/Glu/Pro for Gly or Ser in the DR1 region 1 to 30. M3 substitutes all Asp/Glu residues for Ala in the DR3 region 311 to 345. M4 substitutes all residues apart from Asp/Glu/Pro for Gly or Ser in the DR3 region 311 to 345. M5 substitutes all Asp/Glu residues for Ala in the DR2 region 161-197. **(B)** The diffusion rate measured by FCS of GFP-tagged Cavin1(1-345) DR sequence mutants in lysates after expression in MCF7 cells (lacking endogenous Cavins and Caveolins). N = 3, n = 15-25. Error bars indicate mean \pm SD, **P<0.05, *** P<0.001, ns – not significant **(C)** GFP-tagged Cavin1(1-345) mutants (green) expressed in PC3 cells and immunolabelled with endogenous CAV1 (red). Scale bar = 10 μ m. **(D)** FRAP analysis of Cavin1 (1-345) M4 mutant showing fast recovery of fluorescence in cytosolic droplets and also droplet fusion events (marked by arrow).

Figure 8. Model for the role of Cavin1 DR domains in LLPS and caveola formation.

(A) Structural model of a Cavin1 homotrimeric assembly. The trimeric HR1 coiled-coil domain is derived from the crystal structure of the mouse Cavin1 HR1 domain ¹¹, the UC1 and HR2 domains are modelled as described previously ¹⁰, and the DR domains are modelled as random coil structures (see Methods for further details). The structure is shown in ribbon diagram (top) and with an electrostatic surface representation (bottom). **(B)** Proposed orientation of Cavin1 proteins on the membrane surface, with membrane-binding HR1 and HR2 domains associated with the phospholipid bilayer and negatively-charged DR sequences directed outwards due to electrostatic repulsion. **(C)** Potential role of Cavin1 disordered sequences in membrane curvature generation due to steric crowding. This concept is largely derived from previous studies of other membrane-associated proteins ^{59, 60}. **(D)** Potential role of Cavin1 fuzzy interactions and LLPS in membrane curvature generation.

Supplementary Information

Figure S1. Electrostatic charge distribution and sequence disorder in the Cavin family proteins.

(A) Protein charge plots of human (h) and zebrafish (z) cavin family proteins performed using the Emboss Server (<http://www.bioinformatics.nl/cgi-bin/emboss/charge>) (using standard input parameters and a window width of five amino acid residues). (B) The Cavin1 sequence was analysed using the D2P2 web server¹⁵ for predicted regions of disorder, and also known sites of post-translational modifications.

Figure S2. Schematic representation of protein expression constructs used in this study.

Figure S3. Cavin1 does not undergo LLPS in the absence of crowding agents.

(A) Liquid-liquid phase separation (LLPS) assay with recombinant Ub- and GFP-tagged Cavin1, at different protein and salt concentrations but in the absence of dextran or other crowding agents. (B) At low concentrations, full length Cavin1 still forms liquid droplets, and Cavin1- Δ DR1 still forms coacervates. Cavin1- Δ DR3 is less prone to LLPS at low concentrations compared to the full-length protein.

Figure S4. Localisation of Cavin1 with truncated DR1 and DR2 domains.

(A) Confocal microscopy images of GFP-Cavin1, GFP-Cavin1- Δ DR1 and GFP-Cavin1- Δ DR3 immunolabelled with CAV1 (red) (B) GFP-Cavin1- Δ DR3 (green) associates with microtubules (red) in PC3 cells and disperses to the cytosol and forms liquid droplets after nocodazole treatment. Fluorescence images acquired with a Zeiss Airyscan2 microscope. (C) Cavin1- Δ DR1-GFP with a C-terminal GFP tag shows a similar intracellular accumulation with CAV1 in PC3 cells as the N-terminal GFP-tagged protein (Fig. 5A), suggesting that the GFP tag does not contribute to this phenotype.

Figure S5. Comparison of Cavin1 truncation mutants with endocytic markers.

(A) GFP-tagged Cavin1- Δ DR1 (green) was expressed in PC3 cells, and fixed cells were immunolabelled for CAV1 (blue) and different endocytic markers (red) including EEA1, GM130, LAMP1 and Rab11. Only EEA1 showed significant overlap with the internalised Cavin1- Δ DR1 and CAV1 positive structures. (B) High-resolution images of GFP-tagged Cavin1 and Cavin1- Δ DR1 (green) in PC3 cells compared with EEA1 (magenta) acquired with a Zeiss Airyscan2 microscope. (C) As for (A) but cells expressing GFP-tagged Cavin1(30-392). Cavin1(30-392) accumulates at

intracellular structures with CAV1 and positive for EEA1 labelling similarly to Cavin1- Δ DR1 with the full deletion of the DR1 domain.

Figure S6. Localisation and membrane remodelling by Cavin1(1-345) mutant proteins.

(A) Summary of specific DR domain mutations in Cavin1(1-345) tested for polymer formation and generation of caveolae. (B) GFP-tagged Cavin1(1-345) mutant M1 was expressed in PC3 cells, and fixed cells were immunolabelled for CAV1 (blue) and different endocytic markers (red) including EEA1, GM130, and LAMP1. Like the complete deletion of the residues 1-30 in the Cavin1 DR1 region (Fig. S4C) Cavin1(1-345) mutant M1 shows significant overlap with CAV1 and EEA1 positive internal structures. (C) APEX-GBP labelling of GFP-tagged Cavin1(1-345) mutant M1 shows accumulation and clustering with internal membrane vesicles (arrows). (D) APEX-GBP labelling of GFP-tagged Cavin1(1-345) mutant M4 shows droplet localisation (arrows). (E) Purified Ub-tagged Cavin1(1-345) mutant M4 was mixed with unilamellar Folch liposomes (extruded to 400 nm diameter) and analysed by negative stain EM (1% uranyl acetate). This mutant is able to remodel and tubulate these synthetic membranes, although with a slightly larger diameter than wild-type Cavin or Cavin1(1-345) (Fig. 3).

Figure S7. Gels showing purified recombinant Cavin1 proteins used in this study (A to G), and western blot (H) showing expression of GFP tagged mutants expressed in PC3 cell line probed with anti-GFP antibody. The diffusion time measurements for three dyes performed before session (I)

Movie S1. (related to Fig. 3B).

Cryoelectron tomography (CryoET) of Cavin1-coated membrane tubules. The movies shows a series of images panning through the three-dimensional tomographic volume. Striated protein densities are observed coating the relatively heterogeneous membrane tubules.

Movie S2. (related to Fig. 5B).

GFP-tagged Cavin1- Δ DR3 was expressed in PC3 cells and photobleaching was performed on a small region along microtubules coated with GFP tagged mutant protein. Images were acquired one frame per second.

Movie S3. (related to Fig. 5C).

GFP-tagged Cavin1- Δ DR3 was expressed in PC3 cells and treated with nocodazole (10 μ M). Photobleaching was performed on a small region containing liquid droplets of mutant protein and images were acquired one frame per second.

Movie S4. (related to Fig. 5F).

GFP-tagged Cavin1 and Rab5a-mCherry were co-expressed in PC3 cells and images were acquired one frame per four seconds.

Movie S5. (related to Fig. 5F).

GFP-tagged Cavin1- Δ DR1 and Rab5a-mCherry were co-expressed in PC3 cells and images were acquired one frame per four seconds.

Movie S6. (Related to Fig. 7D).

GFP-Cavin1 M4 mutant expressed in PC3 cell line and photobleaching was performed on protein droplets dispersed in cytosol. Images were acquired one frame per two seconds.

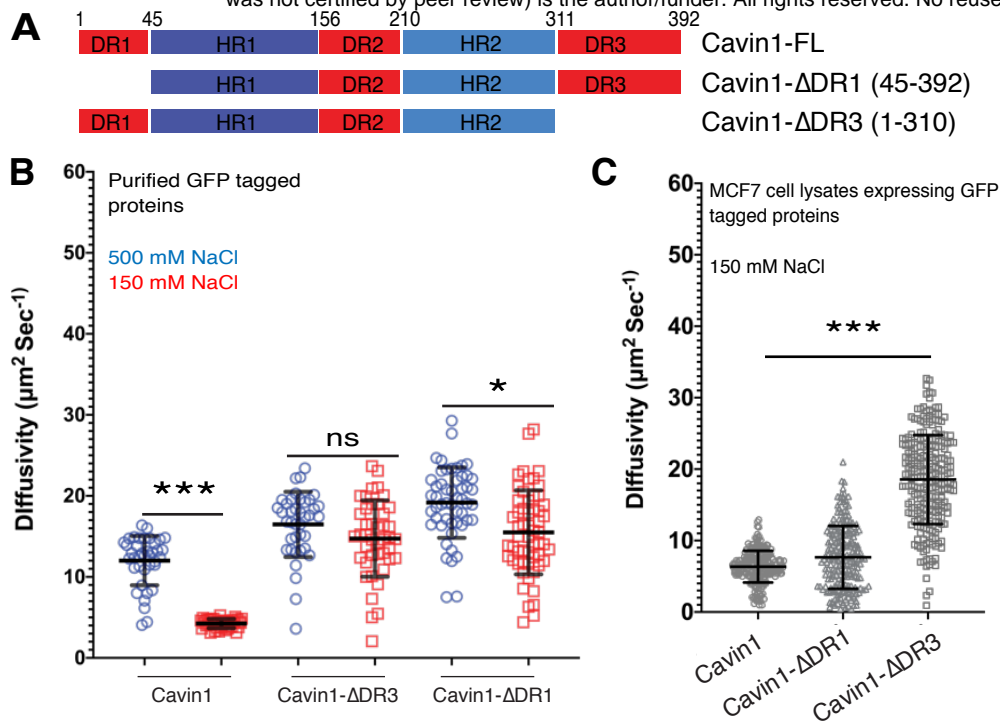
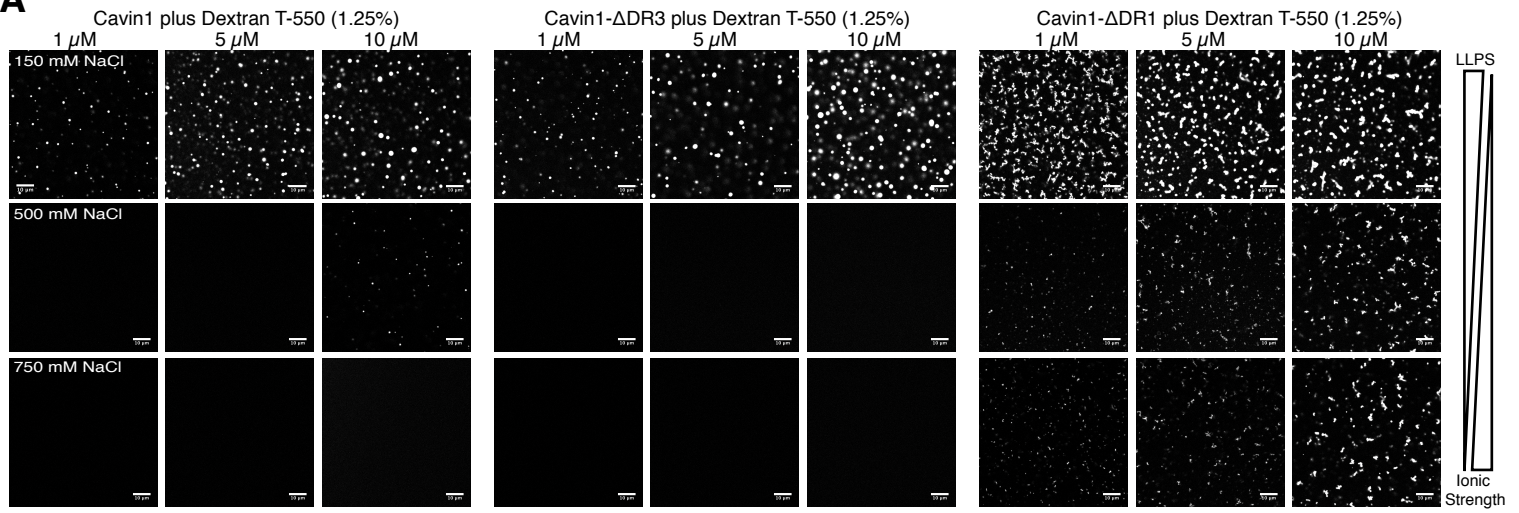


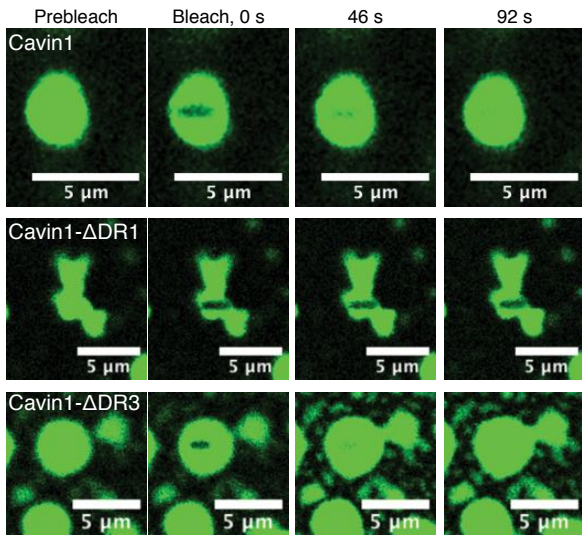
Figure 1. The Cav1 N- and C-terminal DR domains are important for self-association.

(A) Schematic representation of Cav1 and truncations. DR, disordered region; HR, helical region. (B) The diffusion rate of Cav1, Cav1-ΔDR1 and Cav1-ΔDR3 in solution assessed by fluorescence correlation spectroscopy (FCS). Bacterially expressed and purified ubiquitin and GFP tagged proteins (Fig. S2) were analysed in high NaCl concentration (500 mM) and physiological NaCl concentration (150 mM). Error bars indicate mean \pm SD (standard deviation), N=2, n=10-15, ns – not significant, *P<0.05 ***P<0.001. (C) The diffusion rate of GFP-tagged Cav1, Cav1-ΔDR1 and Cav1-ΔDR3 in lysates after expression in MCF7 cells (lacking endogenous Cavins and Caveolins). Buffer contained 150 mM NaCl. N=3, n=20-25, ns – not significant, ***P<0.001. Error bars indicate mean \pm SD.

A



B



C

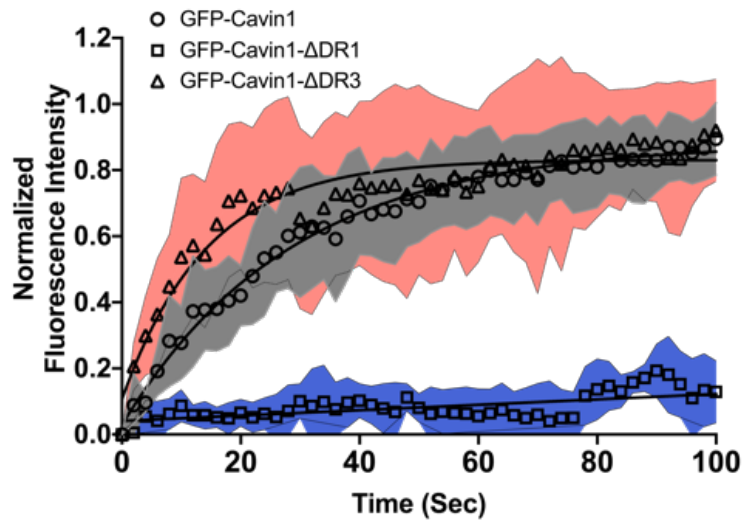


Figure 2. Cav1 undergoes liquid-liquid phase separation in vitro.

(A) Liquid-liquid phase separation (LLPS) assays with recombinant Ub- and GFP-tagged Cav1, Cav1-ΔDR3 and Cav1-ΔDR1 at different protein and salt concentrations. (B) Fluorescence recovery after photobleaching (FRAP) assay with Cav1, Cav1-ΔDR3 and Cav1-ΔDR1 showing GFP fluorescence images at increasing times. (C) Plot of normalized fluorescence intensity after photobleaching. N=6-8, Grey, blue and pink shaded areas around recovery curves represent standard deviation (SD). While Cav1 and Cav1-ΔDR3 droplets rapidly exchange with the bulk solution and recover their fluorescence, Cav1-ΔDR1 shows virtually no exchange indicating gel formation.

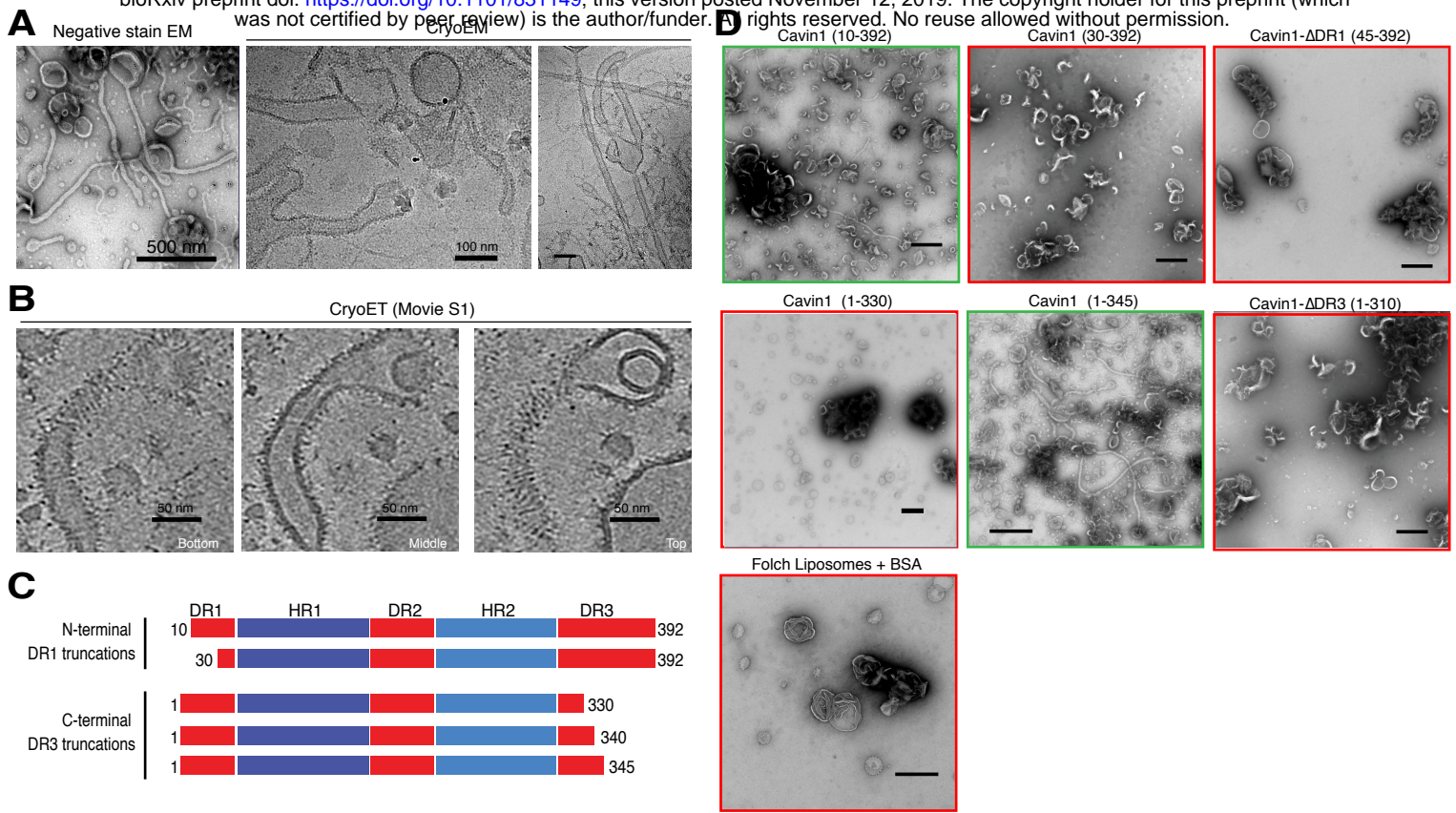
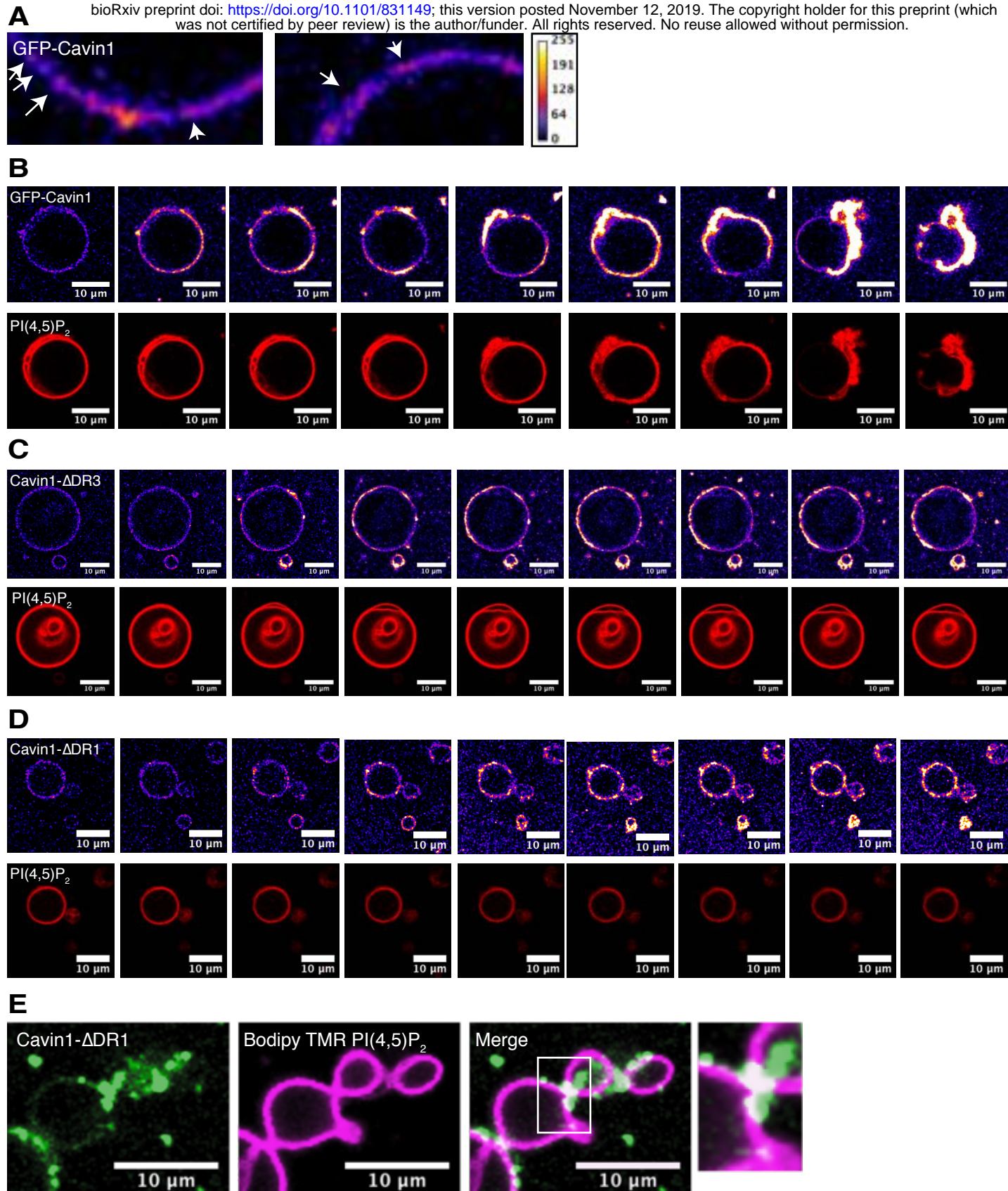


Figure 3. The Cav1 DR domains are required for membrane remodelling in vitro.

(A) Purified Ub-tagged full length Cav1 was mixed with Folch 400 nm unilamellar liposomes and analysed by both negative stain EM (1% uranyl acetate) and cryoEM. (B) Cryoelectron tomography (CryoET) of Cav1-coated membrane tubules showing bottom, middle and top sections of three-dimensional projections. Striated protein densities are observed coating the relatively heterogeneous membrane tubules. The full tomogram is shown in Movie S1. (C) Schematic diagram of Cav1 and different truncation constructs examined for their ability to remodel membranes in vitro. (D) Purified Ub-tagged Cav1 truncations were mixed with Folch 400 nm unilamellar liposomes and analysed by negative stain EM (1% uranyl acetate). Full membrane tubulation and remodelling activity requires residues 1-30 in DR1, and residues 330-345 in DR3.



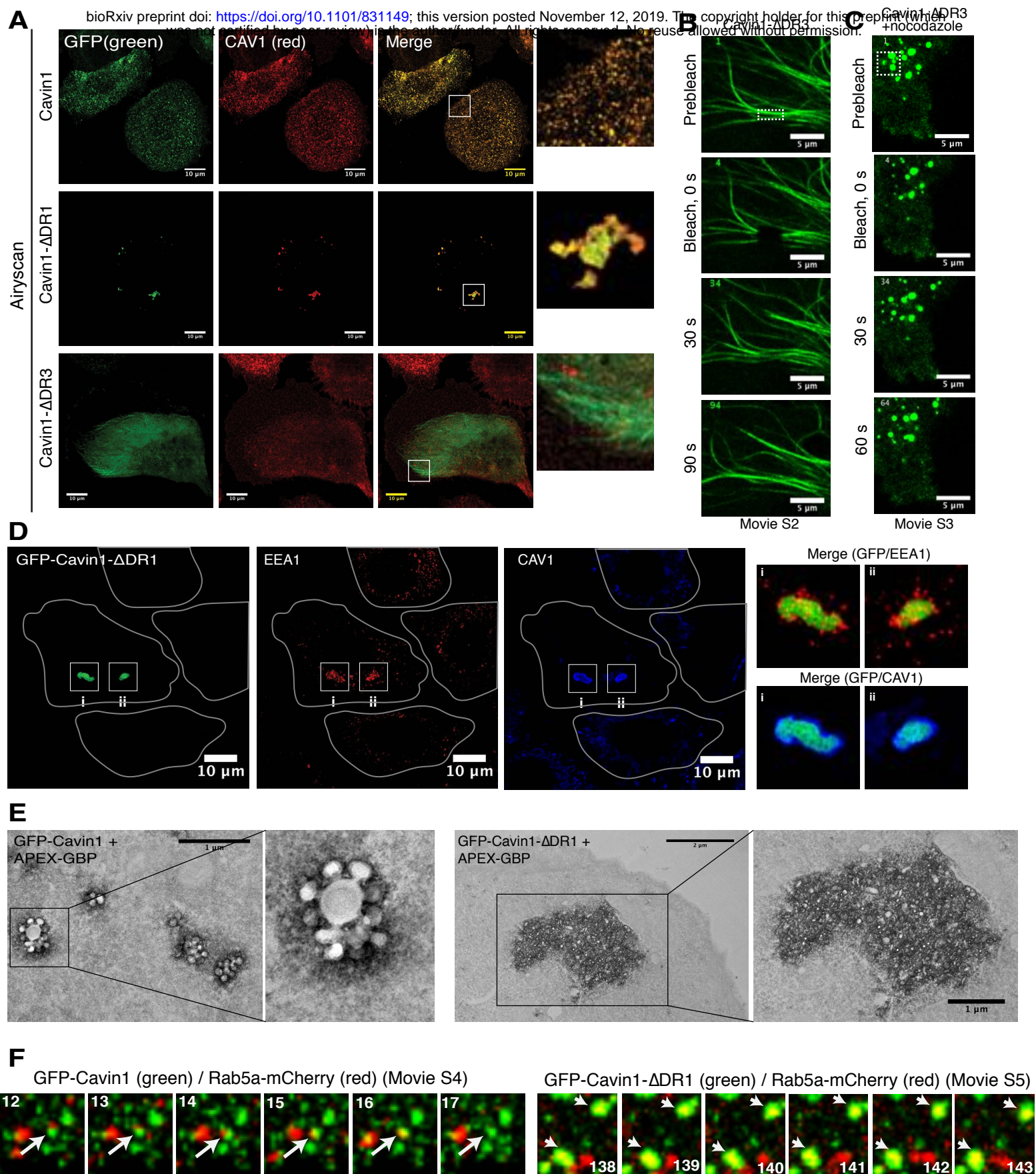


Figure 5. The Cavin1 DR domains are essential for caveola formation with CAV1.

(A) GFP-tagged Cavin1 and truncations (green) were expressed for 24 h in PC3 cells, fixed and immunolabelled for Caveolin1 (CAV1) (red). Full length Cavin1 forms typical caveola puncta, colocalising with CAV1 at the cell surface. Cavin1- Δ DR1 mutant expression leads to formation of tethered intracellular CAV1-positive clusters. Cavin1- Δ DR3 shows cytoplasmic and microtubule localisation. Images were collected using a Zeiss fast Airyscan microscope. Fluorescence recovery after photobleaching (FRAP) analysis of GFP-Cavin1- Δ DR3 before (B) and after (C) nocodazole (10 μ M) addition. (D) In PC3 cells GFP-tagged Cavin1- Δ DR1 truncation shows colocalization with the early endosomal marker (EEA1) (red) and CAV1 (blue). Inset shows merge images of GFP-Cavin1- Δ DR1/EEA1 and GFP-Cavin1- Δ DR1/CAV1. (E) GFP-tagged Cavin1 and Cavin1- Δ DR1 were visualised in PC3 cells by electron microscopy and labelling of GFP tagged proteins using APEX-GBP staining. (F) Live imaging of PC3 cells expressing Rab5a-mCherry with either GFP-Cavin1 or GFP-Cavin1- Δ DR1. Images were acquired one frame per four seconds and frame numbers are indicated in boxes. Arrows indicate mCherry/GFP signal co-localisation or separation event.

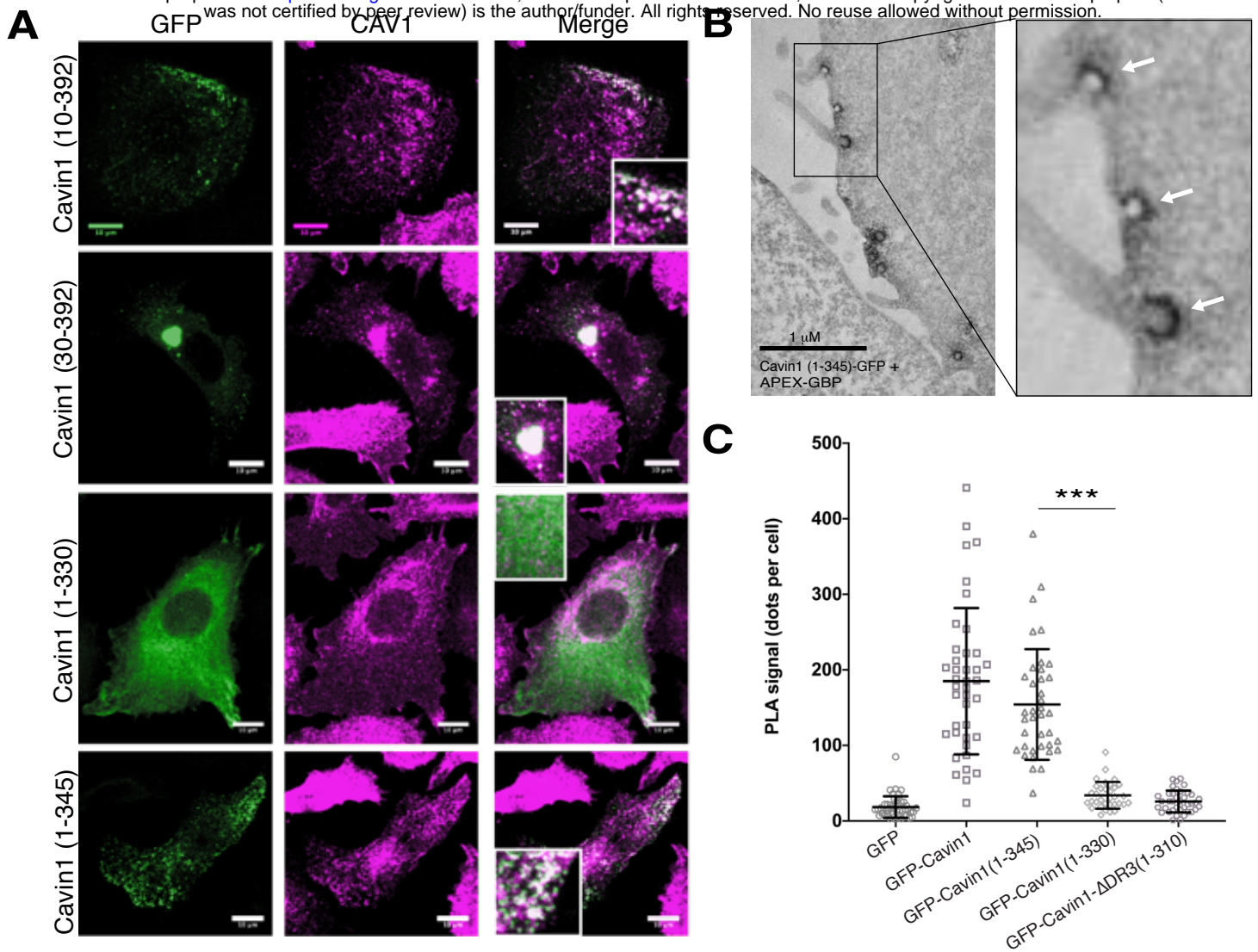


Figure 6. Definition of the minimal DR sequences required for Cavin1 function.

(A) GFP-tagged Cavin1 DR domain truncation mutants (green) (Fig. 3C) were expressed in PC3 cells and immunolabelled with CAV1 (red). Residues 1-30 in DR1 and 330-345 are required for caveola formation. (B) APEX-GBP labelling of GFP tagged Cavin1(1-345) shows normal bulb-shaped caveolae at the plasma membrane. (C) Proximity ligation assay (PLA) analyses show that truncation of Cavin1 from the C-terminus beyond residue 345 results in loss of association with CAV1. PLA signal was quantified as dots per cell for specific interaction between GFP-tagged proteins and CAV1, N = 2 (independent biological replicates), n = 10-15 (cells per replicates), Error bars indicate mean \pm SD, *** P<0.001.

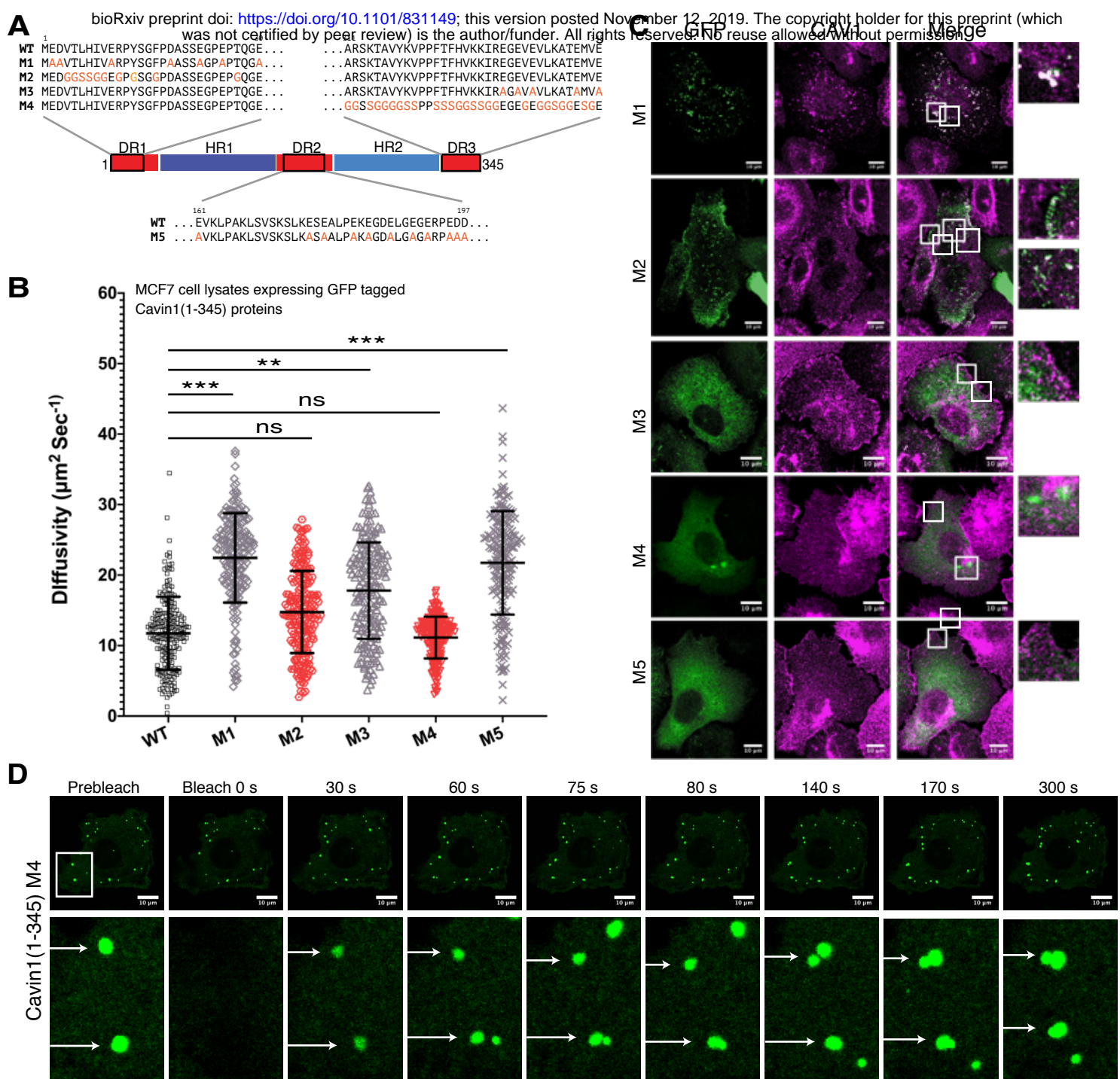


Figure 7. DR-dependent Cav1 higher order polymer formation and caveola assembly.

(A) Schematic diagram of Cav1(1-345) with the sequences of the M1-M5 point mutants indicated. M1 substitutes all Asp/Glu residues for Ala in the DR1 region 1 to 30. M2 substitutes all residues apart from Asp/Glu/Pro for Gly or Ser in the DR1 region 1 to 30. M3 substitutes all Asp/Glu residues for Ala in the DR3 region 311 to 345. M4 substitutes all residues apart from Asp/Glu/Pro for Gly or Ser in the DR3 region 311 to 345. M5 substitutes all Asp/Glu residues for Ala in the DR2 region 161-197. (B) The diffusion rate measured by FCS of GFP-tagged Cav1(1-345) DR sequence mutants in lysates after expression in MCF7 cells (lacking endogenous Cavins and Caveolins). $N = 3$, $n = 15-25$. Error bars indicate mean \pm SD, ** $P < 0.05$, *** $P < 0.001$, ns – not significant (C) GFP-tagged Cav1(1-345) mutants (green) expressed in PC3 cells and immunolabelled with endogenous CAV1 (red). Scale bar = 10 μm . (D) FRAP analysis of Cav1(1-345) M4 mutant showing fast recovery of fluorescence in cytosolic droplets and also droplet fusion events (marked by arrow).

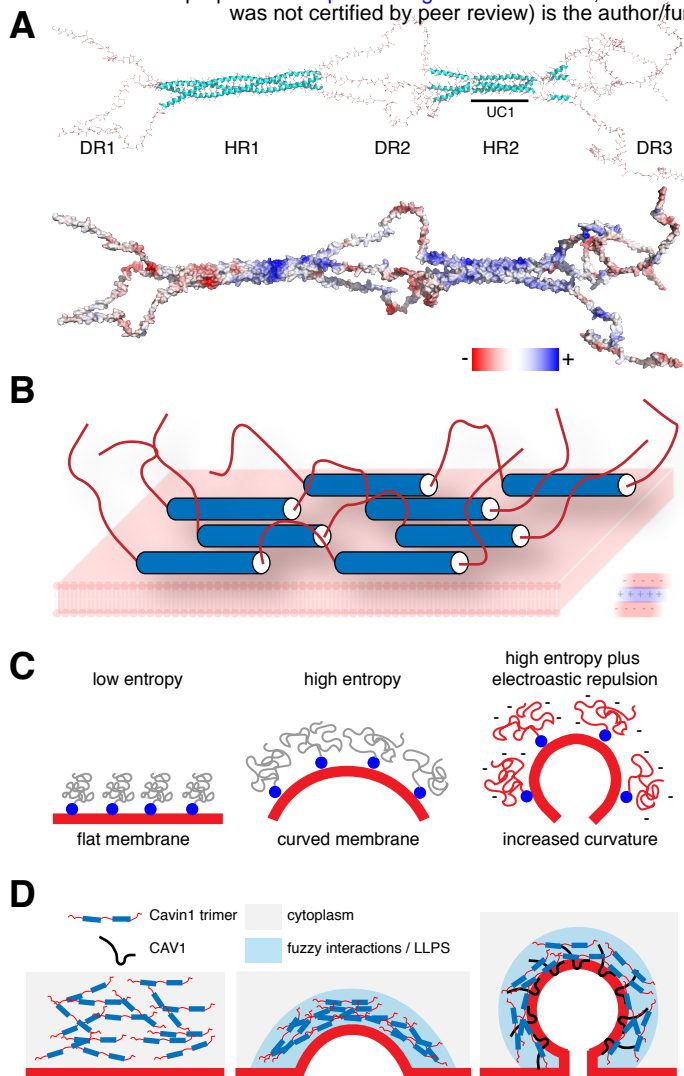
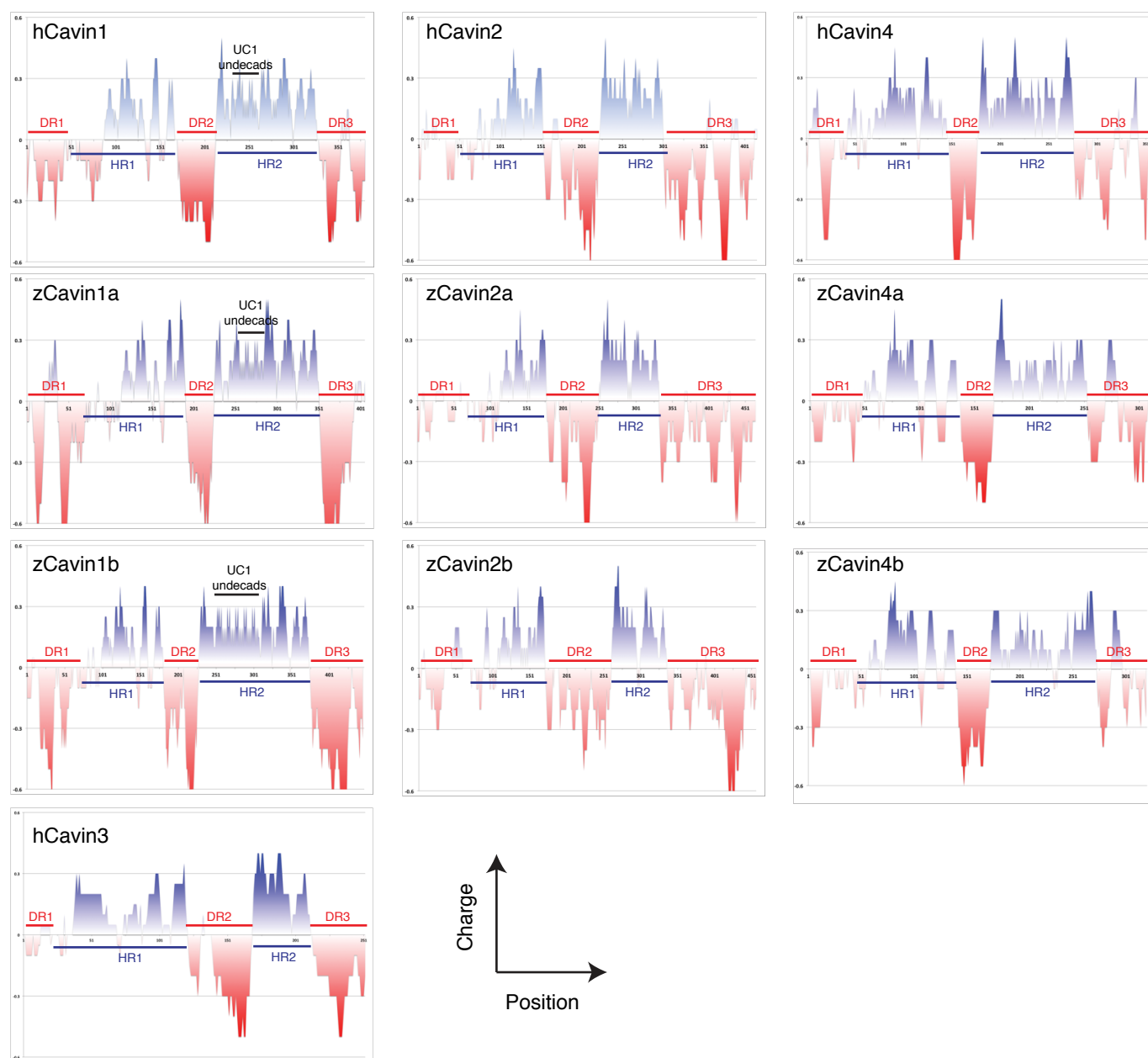


Figure 8. Model for the role of Cavin1 DR domains in LLPS and caveola formation.

(A) Structural model of a Cavin1 homotrimeric assembly. The trimeric HR1 coiled-coil domain is derived from the crystal structure of the mouse Cavin1 HR1 domain 11, the UC1 and HR2 domains are modelled as described previously 10, and the DR domains are modelled as random coil structures (see Methods for further details). The structure is shown in ribbon diagram (top) and with an electrostatic surface representation (bottom). (B) Proposed orientation of Cavin1 proteins on the membrane surface, with membrane-binding HR1 and HR2 domains associated with the phospholipid bilayer and negatively-charged DR sequences directed outwards due to electrostatic repulsion. (C) Potential role of Cavin1 disordered sequences in membrane curvature generation due to steric crowding. This concept is largely derived from previous studies of other membrane-associated proteins ^{57, 58}. (D) Potential role of Cavin1 fuzzy interactions and LLPS in membrane curvature generation.

A



B

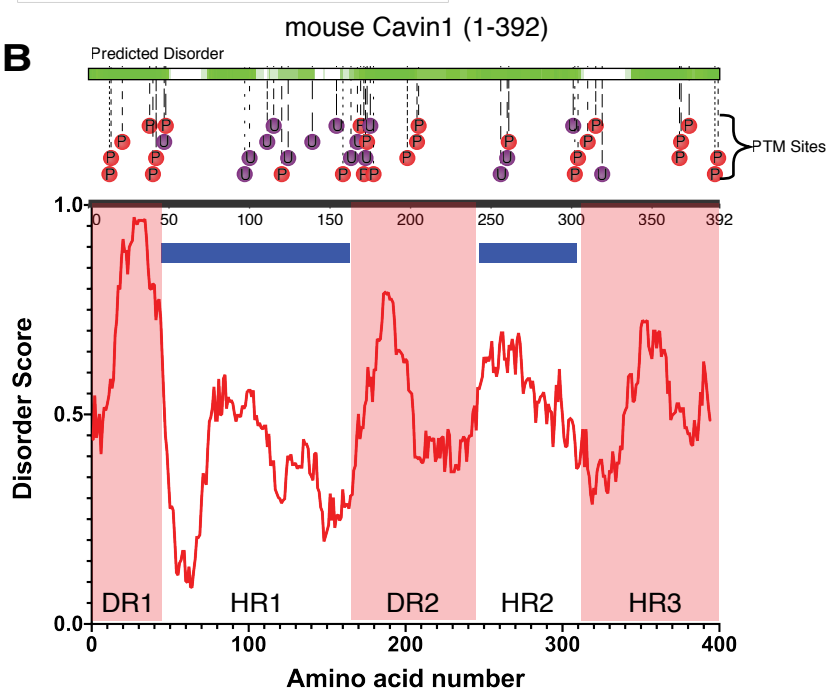
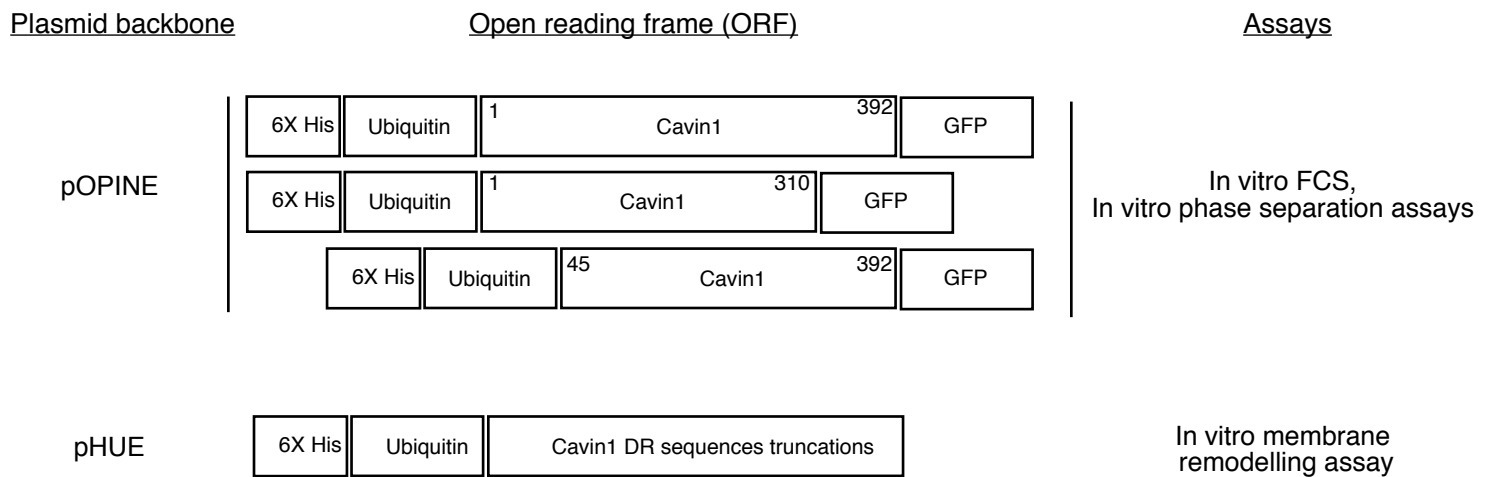


Figure S1. Electrostatic charge distribution and sequence disorder in the Cavin family proteins.

(A) Protein charge plots of human (h) and zebrafish (z) cavin family proteins performed using the Emboss Server (<http://www.bioinformatics.nl/cgi-bin/emboss/charge>) (using standard input parameters and a window width of five amino acid residues). (B) The Cavin1 sequence was analysed using the D2P2 web server 15 for predicted regions of disorder, and also known sites of post-translational modifications.

Mouse Cavin1 bacterial expression constructs



Mouse Cavin1 mammalian expression constructs

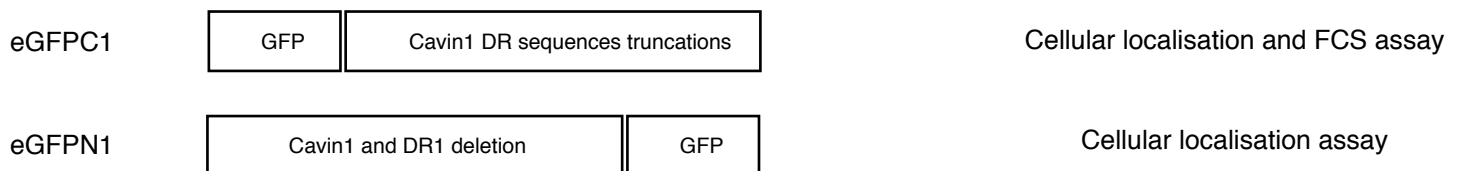
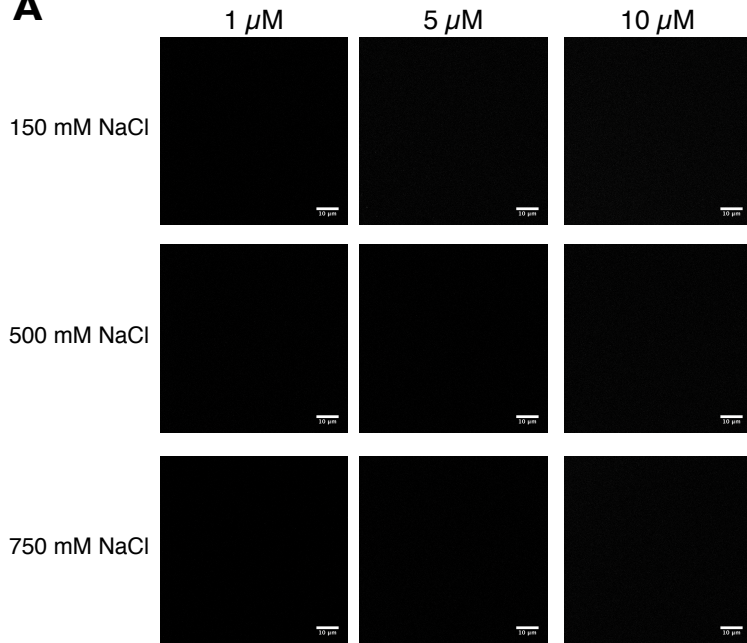


Figure S2. Schematic representation of protein expression constructs used in this study.

GFP-Cavin1 without Dextran -T550 addition

A



B

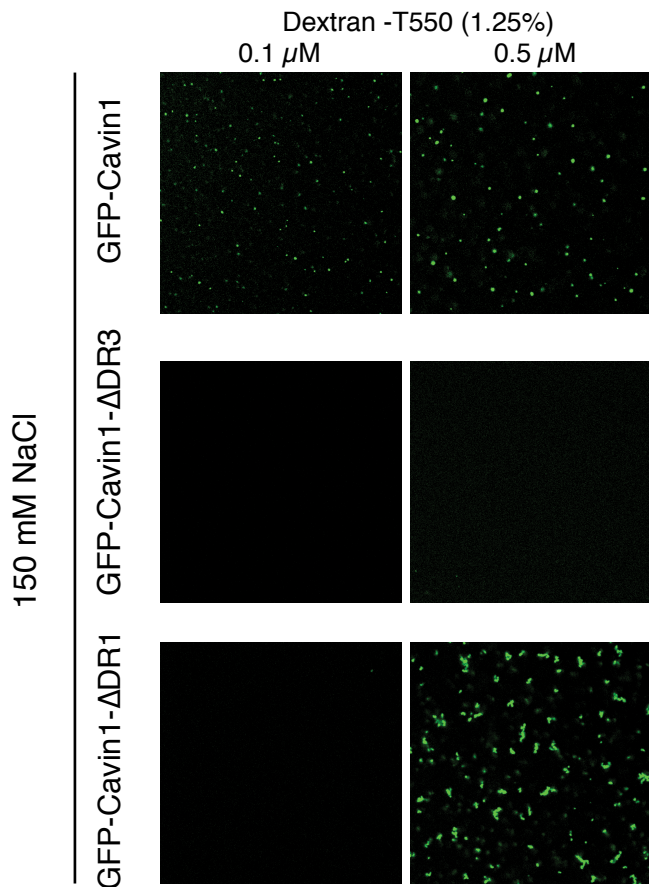
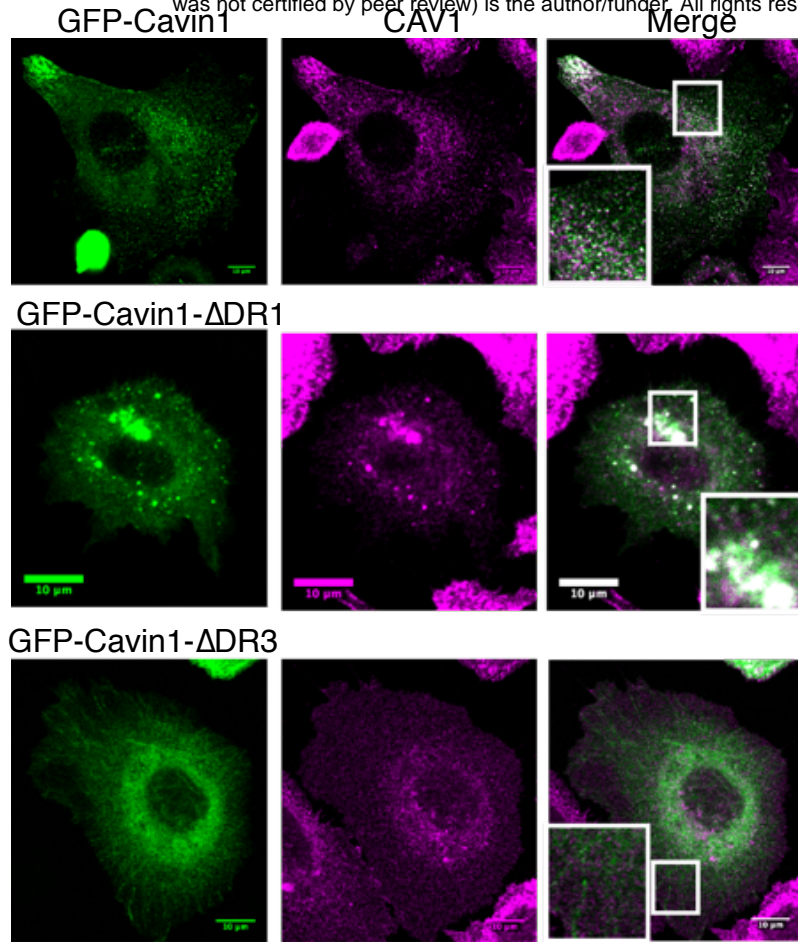


Figure S3. Cavin1 does not undergo LLPS in the absence of crowding agents.

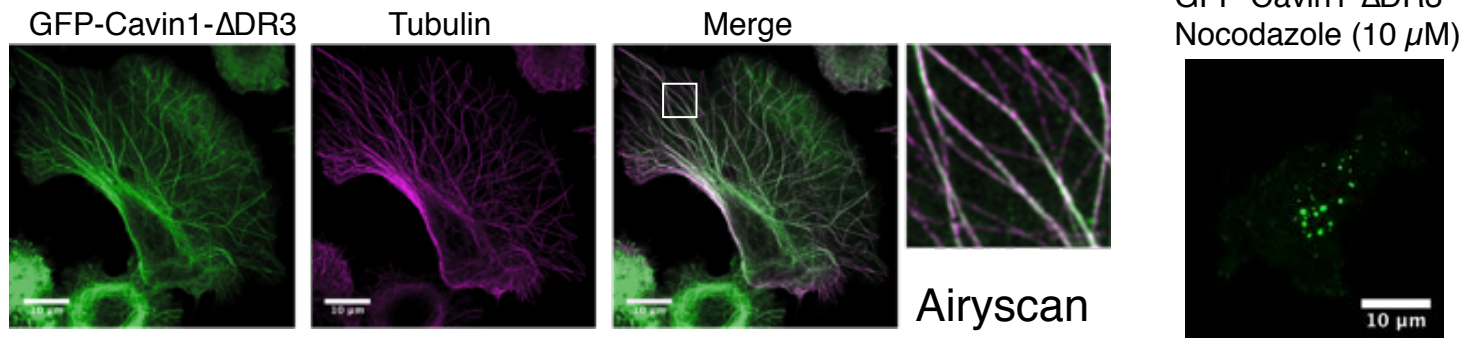
(A) Liquid-liquid phase separation (LLPS) assay with recombinant Ub- and GFP-tagged Cavin1, at different protein and salt concentrations but in the absence of dextran or other crowding agents. (B) At low concentrations, full length Cavin1 still forms liquid droplets, and Cavin1- Δ DR1 still forms coacervates. Cavin1- Δ DR3 is less prone to LLPS at low concentrations compared to the full-length protein.

A

Confocal microscopy



B



C

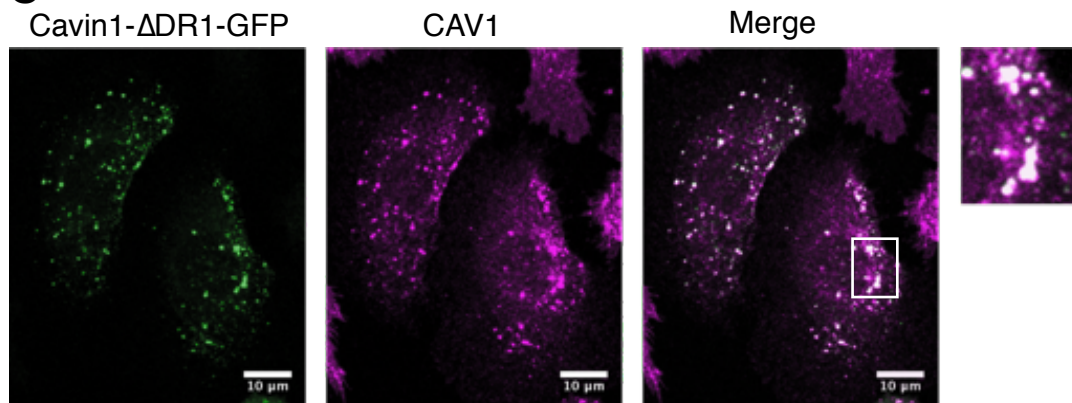


Figure S4. Localisation of Cavin1 with truncated DR1 and DR2 domains.

(A) Confocal microscopy images of GFP-Cavin1, GFP-Cavin1- Δ DR1 and GFP-Cavin1- Δ DR3 immunolabelled with CAV1 (red) (B) GFP-Cavin1- Δ DR3 (green) associates with microtubules (red) in PC3 cells and disperses to the cytosol and forms liquid droplets after nocodazole treatment. Fluorescence images acquired with a Zeiss Airyscan2 microscope. (C) Cavin1- Δ DR1-GFP with a C-terminal GFP tag shows a similar intracellular accumulation with CAV1 in PC3 cells as the N-terminal GFP-tagged protein (Fig. 5A), suggesting that the GFP tag does not contribute to this phenotype.

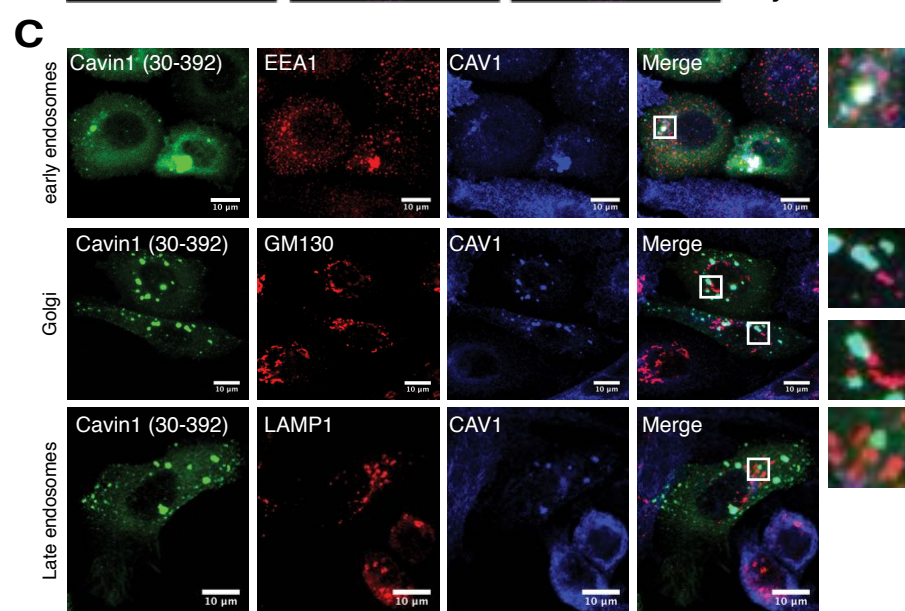
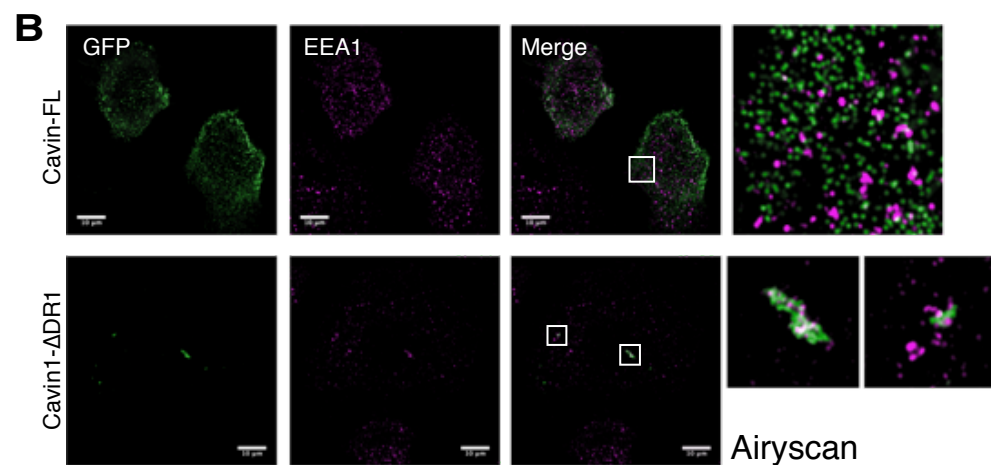
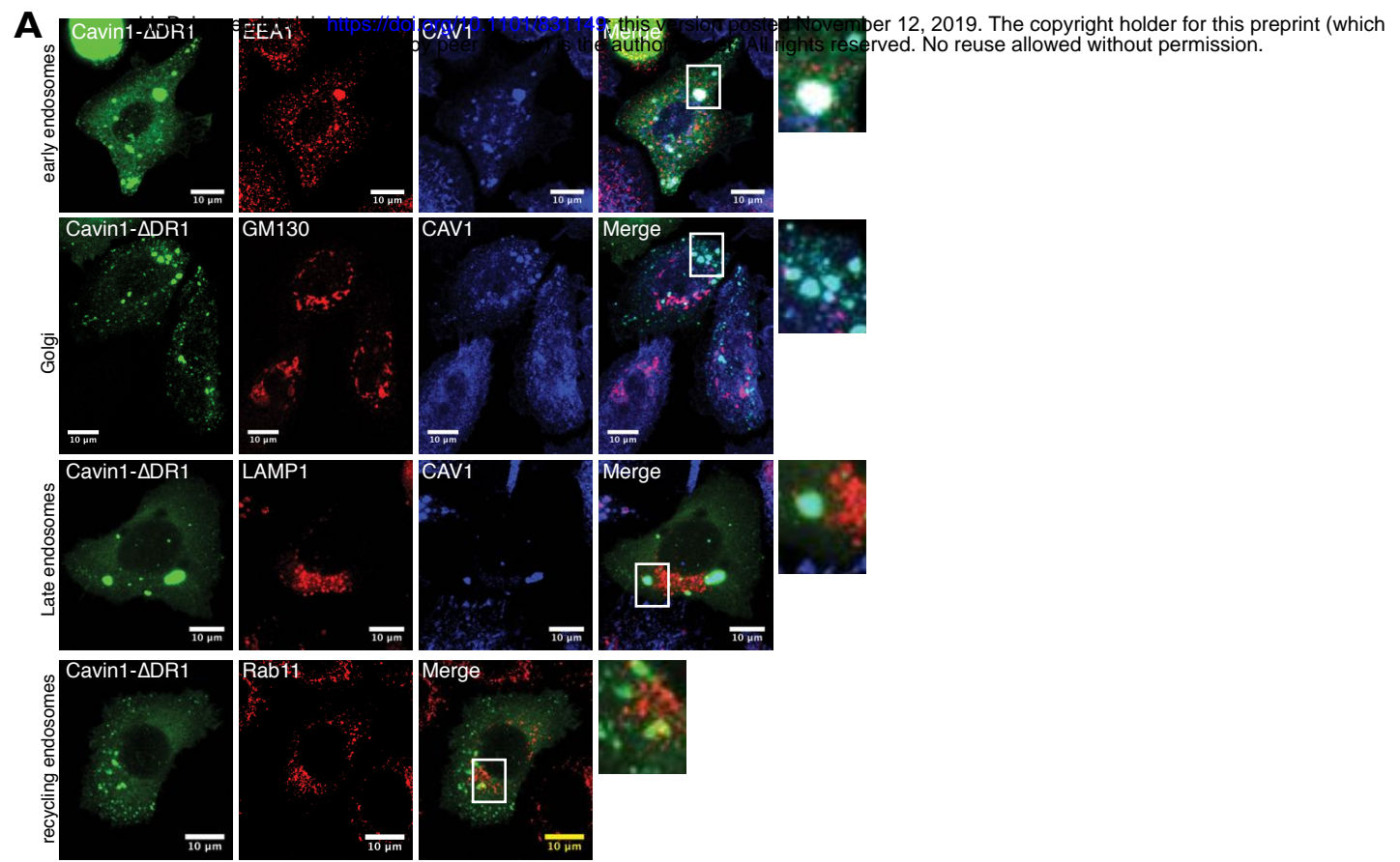


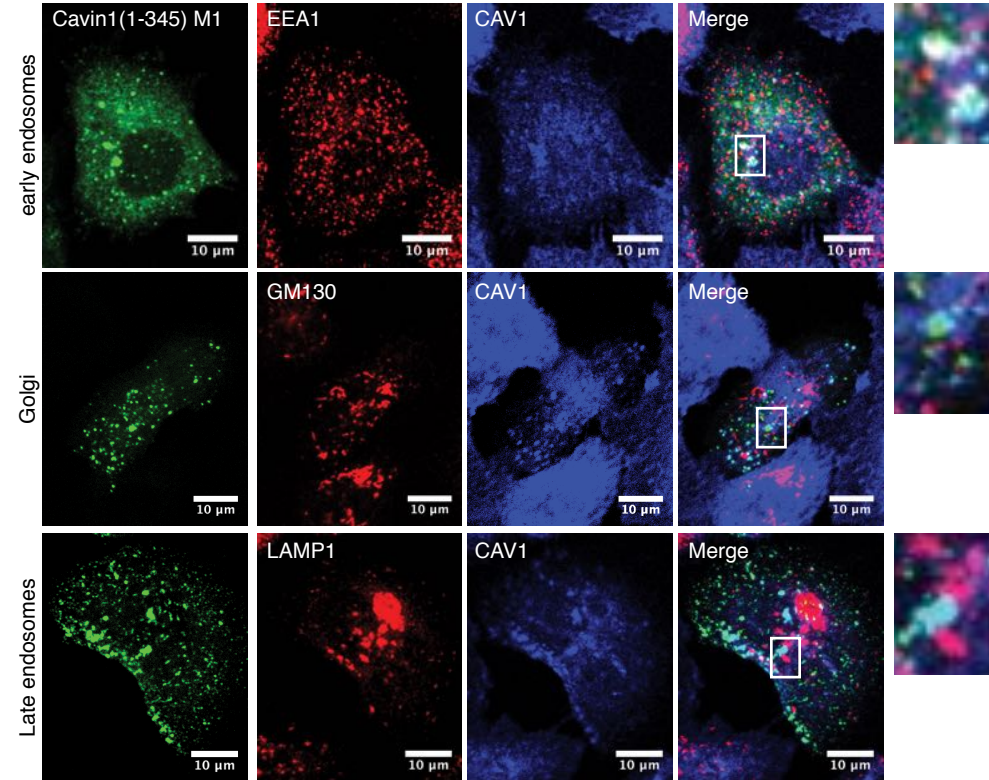
Figure S5. Comparison of Cavin1 truncation mutants with endocytic markers.

(A) GFP-tagged Cavin1- Δ DR1 (green) was expressed in PC3 cells, and fixed cells were immunolabelled for CAV1 (blue) and different endocytic markers (red) including EEA1, GM130, LAMP1 and Rab11. Only EEA1 showed significant overlap with the internalised Cavin1- Δ DR1 and CAV1 positive structures. (B) High-resolution images of GFP-tagged Cavin1 and Cavin1- Δ DR1 (green) in PC3 cells compared with EEA1 (magenta) acquired with a Zeiss Airyscan2 microscope. (C) As for (A) but cells expressing GFP-tagged Cavin1(30-392). Cavin1(30-392) accumulates at intracellular structures with CAV1 and positive for EEA1 labelling similarly to Cavin1- Δ DR1 with the full deletion of the DR1 domain.

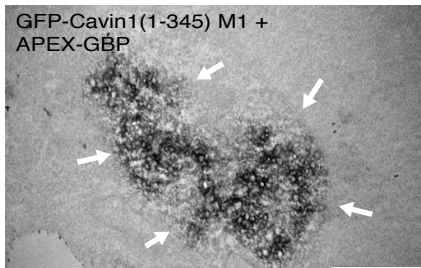
A

Cavin1(1-345) mutants	
M1	N-terminal DR1 (1-30) acidic residues to alanine
M2	N-terminal DR1 (1-30) random GS substitution except acidic residues
M3	C-terminal DR3 (311-345) acidic residues to alanine
M4	C-terminal DR3 (311-345) random GS substitution except acidic residues
M5	Central DR2 (155-200) acidic residues to alanine

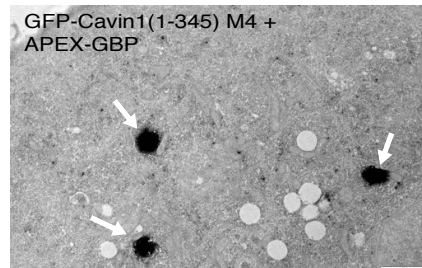
B



C



D



E

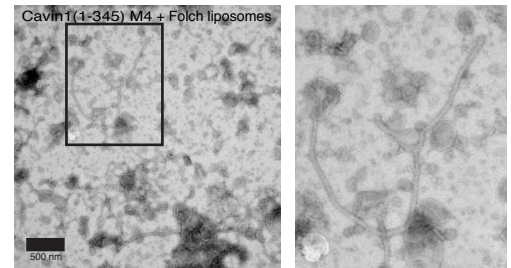


Figure S6. Localisation and membrane remodelling by Cav1(1-345) mutant proteins.

(A) Summary of specific DR domain mutations in Cav1(1-345) tested for polymer formation and generation of caveolae. (B) GFP-tagged Cav1(1-345) mutant M1 was expressed in PC3 cells, and fixed cells were immunolabelled for CAV1 (blue) and different endocytic markers (red) including EEA1, GM130, and LAMP1. Like the complete deletion of the residues 1-30 in the Cav1 DR1 region (Fig. S4C) Cav1(1-345) mutant M1 shows significant overlap with CAV1 and EEA1 positive internal structures. (C) APEX-GBP labelling of GFP-tagged Cav1(1-345) mutant M1 shows accumulation and clustering with internal membrane vesicles (arrows). (D) APEX-GBP labelling of GFP-tagged Cav1(1-345) mutant M4 shows droplet localisation (arrows). (E) Purified Ub-tagged Cav1(1-345) mutant M4 was mixed with unilamellar Folch liposomes (extruded to 400 nm diameter) and analysed by negative stain EM (1% uranyl acetate). This mutant is able to remodel and tubulate these synthetic membranes, although with a slightly larger diameter than wild-type Cavin or Cav1(1-345) (Fig. 3).

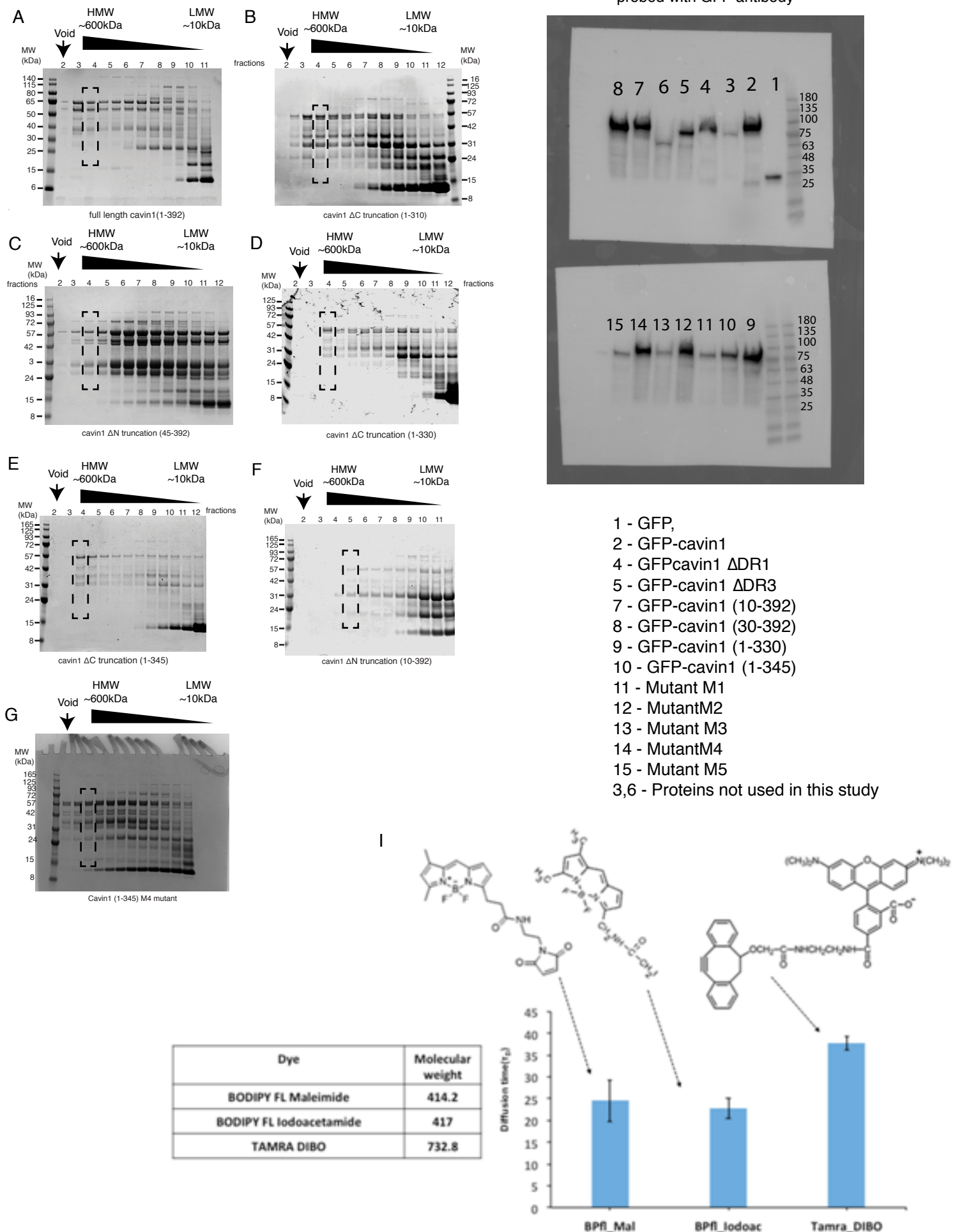


Figure S7. Gels showing purified recombinant Cavin1 proteins used in this study (A to G), and western blot (H) showing expression of GFP tagged mutants expressed in PC3 cell line probed with anti-GFP antibody. The diffusion time measurements for three dyes performed before session (I)